UNIVERSIDAD NACIONAL AUTÓNOMA DE MÉXICO

PROGRAMA DE MAESTRÍA Y DOCTORADO EN INGENIERÍA

ENERGÍA – SISTEMAS ENERGÉTICOS

THERMAL-HYDRAULICS OF SUPER CRITICAL WATER COOLED REACTORS

TESIS

PARA OPTAR POR EL GRADO DE:

MAESTRO EN INGENIERÍA

PRESENTA:

ERICK GILBERTO ESPINOSA MARTÍNEZ

TUTOR PRINCIPAL:

DRA. CECILIA MARTÍN DEL CAMPO MÁRQUEZ

Facultad de Ingeniería-UNAM

COMITÉ TUTOR:

DR. JUAN LUIS FRANÇOIS LACOUTURE, Facultad de Ingeniería-UNAM

DRA. PAMELA FRAN NELSON EDELSTEIN, Facultad de Ingeniería-UNAM

DR. ALEJANDRO NUÑEZ CARRERA, CNSNS

DR. RODOLFO VÁZQUEZ RODRÍGUEZ, UAM-I

Ciudad Universitaria, Cd. Mx., ENERO 2017

JURADO ASIGNADO:

Presidente:	Dr. François Lacouture Juan Luis
Secretario:	Dra. Nelson Edelstein Pamela Fran
1er Vocal:	Dra. Martín del Campo Márquez Cecilia
2do Vocal:	Dr. Núñez Carrera Alejandro
2do Vocal:	Dr. Vázquez Rodríguez Rodolfo

Lugar o lugares donde se realizó la tesis:
UNIVERSIDAD NACIONAL AUTÓNOMA DE MÉXICO
FACULTAD DE INGENIERÍA

TUTOR DE TESIS:

CECILIA MARTÍN DEL CAMPO MÁRQUEZ

FIRMA

Nicolás

Mérida

ACKNOWLEDGMENTS

I wish to thank to my family, for their support, and especially my parents who have never turn their back on me.

I thank my Tutorial Committee for their support and their time; especially to my thesis director, Dra. Cecilia Martín del Campo Márquez.

To all my professors, who have shared their knowledge and have challenged me to give all my effort.

To The National Autonomous University of Mexico (UNAM) for giving me the chance to perform my postgraduate studies.

To CONACyT for the schorlarship granted in order to be able to perform my studies full time.

Abstract

In this Master's Thesis the numerical analysis of the thermal-hydraulics behavior of the High Performance Light Water Reactor (HPLWR), the European version of a supercritical water reactor (SCWR) with reduced order models, is presented. The thermal-hydraulics analysis considers a three-pass core design with multiple heat-up steps. Each pass was simulated with a model using an average channel. The neutronic calculations were performed with HELIOS-2 and the obtained results were used to evaluate the reactivity feedback, caused by changes in fuel temperature and supercritical water density, which was used in the point kinetics model. The core thermal-hydraulics behavior was analyzed for the steady state and for some transients by means of models with and without temperature feedback effects. An accurate understanding of the heat transfer correlations on the prediction of the fuel temperature could provide important insights for improving the safety and the performance of the SCWRs. A discussion and comparison of the results obtained with different correlations was carried out and presented. Additionally the sensitivity and uncertainty analysis of a SCWR applying a methodology based on Monte Carlo with reduced order models is presented. The Monte Carlo's methodology was applied systematically to establish the operating domain, due that SCWRs are not yet in operation, and the analysis of the nuclear and thermal–hydraulic processes must rely on numerical modeling with the purpose of developing or confirming the design basis. The methodology considers an invariability test to obtain the representative sample, i.e., invariable results with the simulation size. The relative standard deviation is calculated and presented for power, temperature and pressure drop, as well as the regression analysis.

INDEX

Figures Index

Tables Index

Nomenclature

ρ	*Density* $\left(\mathrm{kg/m^3}\right)$
Cp	*Heat capacity* $\left(\mathrm{J/kg \cdot K}\right)$
T	*Temperature* $\left(\mathrm{K}\right)$
t	*Time* $\left(\mathrm{s}\right)$
r	*Radius* $\left(\mathrm{m}\right)$
q''	*Heat flux* $\left(\mathrm{W/m^2}\right)$
q'''	*Volumetric heat flux* $\left(\mathrm{W/m^3}\right)$
k	*Thermal conductivity* $\left(\mathrm{W/m \cdot K}\right)$
H_∞	*Convective heat transfer coefficient* $\left(\mathrm{W/m^2 \cdot K}\right)$
P	*Neutronic power* $\left(\mathrm{W}\right)$
V	*Volume* $\left(\mathrm{m^3}\right)$
D_e	*Equivalent hydraulic diameter* $\left(\mathrm{m}\right)$
D_h	*Hydraulic diameter* $\left(\mathrm{m}\right)$
μ	*Viscosity* $\left(\mathrm{Pa \cdot s}\right)$
h	*Enthalpy* $\left(\mathrm{J/kg}\right)$
f	*Friction factor*
P_H	*Heated perimeter* $\left(\mathrm{m}\right)$
A_f	*Flow area* $\left(\mathrm{m^2}\right)$
d_{ex}	*External diameter* $\left(\mathrm{m}\right)$
g	*Gravity*

P	*Pitch*
Δz	*Axial node length*
G	*Mass flux* $\left(\mathrm{kg}/\mathrm{m}^2 \cdot \mathrm{s}\right)$

Subindexes

0	*Center*
cl	*Cladding*
f	*Fuel*
g	*Gap*
j	*Node number*
w	*Wall*
b	*Bulk*

Adimensional Numbers

Nu	*Nusselt number*
Pr	*Prandtl number*
Re	*Reynolds number*

CHAPTER I

INTRODUCTION

The HPLWR (High Performance Light Water Reactor) is the European version of the SCWR (Supercritical Water Cooled Reactor) concept, which is one of the promising future reactor concepts of the Generation IV International Forum (GIF). The main difference between the SCWR and the current light water reactors (LWR) is its operating condition at a higher pressure beyond the critical point of water (25 MPa), as well as, a heat-up of the coolant within the core which is also greater, thus, reaches higher core outlet temperatures (the water enters the core at 553K and leaves above 773K). This leads to a significant increase in the turbine´s power and thermal efficiency of the power plant. For this reason some components of the current light water reactors are not necessary in the SCWR, such as steam separators and dryers, steam generators, a pressurizer, and primary loop pumps. Due to the supercritical conditions of water, the supercritical coolant could be modeled as a single-phase fluid, because water does not exhibit a change of phase from liquid to gas at supercritical pressure conditions, so a boiling crisis cannot occur during the heat-up process in the SCWR core. A thermodynamic steam cycle of such reactors can be derived from supercritical modern fossil fired power plants, however, the reactor itself, and in particular the reactor core, still need to be studied. Due to the significant changes in the physical properties of water, at supercritical pressure, the system is susceptible to local oscillations of temperature, density and power. Strong variations in the vicinity of the pseudo-critical line result in unusual heat transfer behavior.

Previous works have contributed to the understanding of the thermal-hydraulic phenomena in the HPLWR (e.g., Renz and Bellinghausen, 1986; Dobashi et al. 1998; Cheng and Schulenberg, 2001; Pioro and Duffey 2007; Cheng et al. 2007; Gu et al. 2008; Gallaway et al., 2008; Hongzhi et al., 2009; Zhu et al., 2013; Espinosa-Martínez et al., 2015). Renz and Bellinghausen (1986) showed that a heat transfer enhancement occurs at low heat fluxes and at a bulk fluid temperature close to the pseudo-critical region, which is mainly due to the increase in the specific heat capacity. Dobashi et al. (1998) compared two different flow directions (upward and downward) of the moderator within the water rods of a hexagonal fuel assembly. These authors found that a downward flow of moderator water can flatten the high density of the power variation in the core. On the other hand, Cheng and Schulenberg (2001) and Pioro and Duffey (2007) observed that a heat transfer enhancement can occur at both high mass and at a relatively low heat fluxes, however, deterioration in the heat transfer was observed at low mass flux and relatively high heat flux, for the same region and for a circular geometry. For the square annular geometry with a helical wire-wrapped spacer, Hongzhi et al. (2009) shared the same observations. Zhu et al. (2013) performed a comparative study of transient flow characteristics and the safety performance for SCWRs with different flow path designs. Other works analyzed the heat transfer in supercritical water using Computational Fluid Dynamics (CFD) (Cheng et al. 2007; Gu et al. 2008; Gallaway et al., 2008). Recently, Espinosa-Martínez et al. (2015) performed a numerical analysis using various heat transfer correlations to evaluate the effect on the prediction of fuel temperatures in SCWRs, and the Swenson's correlation gave the most conservative predictions, in terms of safety, because higher temperatures were calculated due to the use of the wall temperature for the Re and Pr calculations, while the other correlations use the bulk temperature.

In order to achieve higher outlet coolant temperatures, and thus a higher specific turbine power and a higher net efficiency, Schulenberg and Starflinger (2007) proposed the application of the concept of supercritical fossil fired power plants as well as to include a second superheater, resulting in the three-pass core concept of a HPLWR, which is analyzed in this paper, whereby each pass was simulated using an average channel. The core thermal-hydraulic behavior has been analyzed in both steady state and transients, with and without temperature feedback effects. The heat transfer correlations on the prediction of the fuel temperatures are discussed. Neutronic calculations were performed with the HELIOS-2 code, and the obtained results were used to evaluate the reactivity feedback controls caused by changes in the fuel temperature and supercritical water density, used in the point kinetics model which was coupled to the thermal-hydraulics model.

CHAPTER II

MATHEMATICAL MODEL

The mathematical model for the HPLWR core was divided into three steps: the heat transfer model in the fuel rod, the thermal-hydraulic model, and the neutronic process model.

2.1. Heat Transfer Model

The simulation of the heat transfer process in the fuel rod of the SCWR was obtained using the numerical model of Espinosa-Paredes and Espinosa-Martínez (2009). The supercritical water reactor was made up of cylindrical fuel rods that contain ceramic pellets inside the metallic tubes or cladding.

A detailed multi-node fuel pin model was developed for this study. The fuel assembly temperature distribution was obtained at each radial node of the 21 hydraulic axial nodes in the core. Two radial nodes were used for the cladding and the gap, two nodes for the evaluation of the boundary conditions, and four nodes for the fuel pin.

The fuel heat transfer was based on the following fundamental assumptions: (i) Axis-symmetric radial heat transfer, ii) heat conduction in the axial direction is negligible compared to the heat conduction in the radial direction, iii) the volumetric heat rate generation in the fuel is uniform in each radial node, and iv) storage of heat in the fuel cladding and gap is negligible.

Under these assumptions, the transient temperature distribution in the fuel pin (2.1), initial condition (2.2) and boundary conditions (2.3, 2.4) are given by,

$$(\rho Cp)\frac{\partial T}{\partial t} = k\frac{1}{r}\frac{\partial}{\partial r}\left(r\frac{\partial T}{\partial r}\right) + q'''(t) \qquad \text{at} \qquad r_0 \le r \le r_{cl} \qquad (2.1)$$

$$\text{I.C.} \quad T(r,0) = T(r) \qquad \text{at} \qquad t = 0 \qquad (2.2)$$

$$\text{B.C.1} \quad -k\frac{\partial T}{\partial r} = H_\infty\left(T - T_m\right) \qquad \text{at} \qquad r = r_{cl} \qquad (2.3)$$

$$\text{B.C.2} \quad \frac{\partial T}{\partial r} = 0 \qquad \text{at} \qquad r = r_0 \qquad (2.4)$$

In these equations, r is the cylindrical radial coordinate, r_0 and r_{cl} are defined in **Fig. 2.1**, $q'''(t) = P(t)/V_f$ at each axial node, where P is the neutronic power, T_m is the coolant temperature, and H_∞ is the convective heat transfer coefficient.

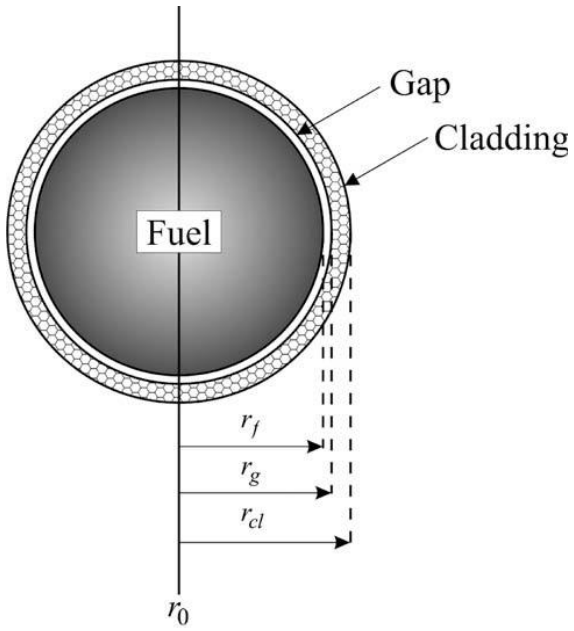

Figure 2.1. Fuel element geometry used in this study.

where $r_f = 3.45\times10^{-3}$ m, $r_g = 3.55\times10^{-3}$ m and $r_{cl} = 4.00\times10^{-3}$ m.

The differential equations described previously are transformed into discrete equations using the control volume formulation technique in an implicit form (Patankar, 1980) for the fuel pin, gap and cladding,

$$a_j T_{j-1}^{t+\Delta t} + b_j T_j^{t+\Delta t} + c_j T_{j+1}^{t+\Delta t} = d_j \tag{2.5}$$

where $T_{j-1}^{t+\Delta t}$, $T_j^{t+\Delta t}$ and $T_{j+1}^{t+\Delta t}$ are unknowns, a_j, b_j, c_j and d_j are coefficients, which are computed at the time t. When these equations are put into a matrix form, the coefficient matrix is tri-diagonal whose solution procedure is the Thomas algorithm, which is the most efficient for

these type of matrices.

The heat transfer coefficient is calculated with the Swenson et al. (1965) correlation,

$$\mathrm{Nu}_b = 0.00459\mathrm{Re}_w^{0.923}\left\langle \mathrm{Pr}_w \right\rangle^{0.613}\left(\frac{\rho_w}{\rho_b}\right)^{0.231} \tag{2.6}$$

where Nu $(=H_\infty/k\,D_e$; H_∞ is the heat transfer coefficient, k is the thermal conductivity and D_e is the hydraulic diameter equivalent), is the Nusselt number; Re $(=G\,D_h/\mu$; G is the mass flux, μ is the viscosity) is the Reynolds number; Pr $(=Cp\,\mu/k$; Cp is the specific heat) is the Prandtl number; and ρ is density; subscripts w and b, denote wall and bulk, respectively.

Espinosa-Martínez et al. (2016) conducted a numerical analysis and found Eq. (2.6) to present the best results among several Heat Transfer Correlations (HTC), including the classical correlation given by Dittus and Boelter (1930), which is widely used for calculations for non-super critical water; additionally Wang and Li (2014) found Eq. (2.6) matches closely to experimental data. Later, a numerical analysis of HTC is presented.

The interaction of the convective heat transfer coefficients with the fuel heat transfer model is brought about through the evaluation of the clad temperature $T\big|_{r=r_{cl}}$. The convective heat transfer coefficient ($H_{¥}$) is used in the boundary condition given by Eq. (2.3), which represents the heat transfer from the wall to the coolant (Eq. 2.9***).***

2.2. Thermal-hydraulic Model

The basic equations to describe the thermal hydraulic behavior in the representative three heated channels (one channel for each pass core), assuming the supercritical fluid is a single phase fluid, are presented in this section.

In this study the flow is considered to be incompressible, i.e., mass flux (G) is a constant. Under this consideration, the energy equation at steady state is given by,

$$\frac{\partial(\rho h)}{\partial t} + G\frac{\partial h}{\partial z} = \frac{q'' P_H}{A_f} + \frac{G}{\rho}\left(\frac{\partial p}{\partial z} + \frac{f G^2}{2 D_h \rho}\right) \tag{2.7}$$

where h is the enthalpy, f is the friction factor, P_H is the heated perimeter, $A_f = P^2 - \pi/4 d_{ex}^2$ is the flow area (where P is the pitch and d_{ex} is the external diameter 2 of the cladding) and $D_h = 4A_f/\pi d_{ex}$ is the hydraulic diameter. This equation is simplified taking into account that the second term on the right side is negligible compared to the term $q''P_H/A_f$. Then Eq. (2.7) becomes,

$$\rho Cp\frac{\partial T}{\partial t} + GCp\frac{\partial T}{\partial z} = \frac{q'' P_H}{A_f} \tag{2.8}$$

The heat transfer from the wall to the coolant is obtained with Newton's law of cooling,

$$q'' = H_{\infty}\left(T_w - T_{\infty}\right) \tag{2.9}$$

The temperature in each node of the channel is obtained numerically as follows,

$$t_j^{t+\Delta t} = T_j^t + \left(\frac{dT}{dt}\right)_j \Delta t \tag{2.10}$$

Where,

$$\left(\frac{\partial T}{\partial t}\right)_j = \frac{1}{\rho Cp}\left(\frac{q'' P_H}{A_f}\right)_j - \frac{G}{\rho Cp}\left(\frac{T_{j+1}^t - T_j^t}{\Delta z}\right) \tag{2.11}$$

where Δz is the node length and j is the node number. The arrangement of the computational nodes of the thermal-hydraulic model is illustrated in **Fig 3.3**.

Additionally, the included time dependent momentum equation is,

$$\frac{\partial G}{\partial t} + \frac{\partial}{\partial z}\left(\frac{G^2}{\rho}\right) = -\frac{\partial p}{\partial z} - \frac{f\,G^2}{2\rho\,D_h} - g\rho \tag{2.12}$$

where f is the friction factor, G is the mass flux, ρ is density, D_h is the hydraulic diameter, g is gravity which can be positive or negative depending on the direction of the fluid, the first term

on the right side is the pressure drop due to acceleration of flow, the second term on the right side is the pressure drop due to frictional resistance and the last term on the right side is the pressure drop due to gravity.

The friction factor, given by Mikheev (1956) is a function of the Reynolds and Prandtl numbers,

$$f = \left(\frac{1}{\left(1.82 \log_{10} \mathrm{Re}_b - 1.64\right)^2} \left(\frac{\mathrm{Pr}_w}{\mathrm{Pr}_b} \right)^{1/3} \right) \tag{2.13}$$

where subscripts w and b, denote wall and bulk, respectively.

The solution of Eq. (2.12) is solved numerically similar as Eq. (2.7),

$$\frac{dp_a}{dz} = \sum_{i=1}^{21} \left[\left(\frac{G^2}{r} \right)_{i-1} - \left(\frac{G^2}{r} \right)_i \right] \frac{1}{\Delta z} \tag{2.14}$$

$$\frac{dp_f}{dz} = \sum_{i=1}^{21} \frac{f G^2}{2 r_i D_h} \tag{2.15}$$

$$\frac{dp_g}{dz} = - \sum_{i=1}^{21} r_i g \tag{2.16}$$

where Eqs. (2.15-2.16) represent the contributions of pressure drop due to acceleration of flow, friction and the entrance and exit of each channel, and gravity, respectively.

CHAPTER III

IMPLEMENTATION

Each channel in the core was based on an hydraulic unit cell whose parameters are: $P_H = 0.025$ m, $D_H = 0.054$ m, and $A_f = 0.34$ m^2. The parameters of the fuel element are: $r_f = 5.207\text{x}10^{-3}$ m for the fuel, $r_g = 5.321\text{x}10^{-3}$ m for the gap, and $r_{cl} = 6.134\text{x}10^{-3}$ m for the clad. The active height of the fuel cell (4.0 m) was divided into 21 equidistant axial nodes ($\Delta z = 0.2$ m). The axial power distribution for each channel was imposed with the idea that the heat flux is not uniform (**Fig. 3.1**).

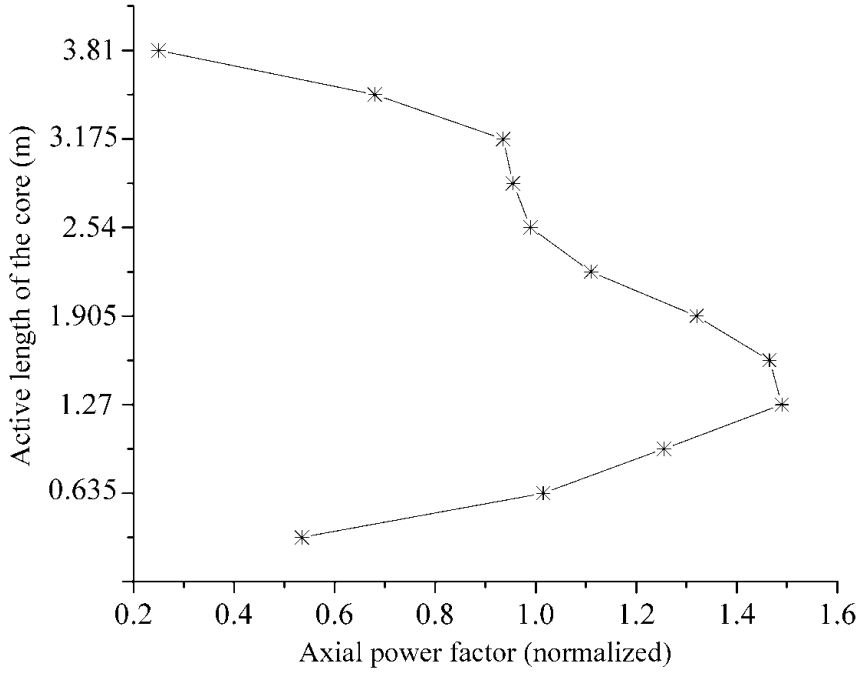

Figure 3.1. Axial power distribution used for the simulations (Reiss et al., 2008).

The thermal physical properties used were taken from Wagner and Kretzschmar (2008). 73, 48 and 35 assembly clusters for Channel 1, Channel 2 and Channel 3, respectively, were used in the simulation, in order to reach a better power distribution within the core.

3.1. Core Design

The SCWR under study is called the three-pass core concept. Water, as working fluid, is guided three times through the core (twice up and once down). The first pass, called the "evaporator", is situated in the center of the core. The evaporator heats the coolant up to 663K, flowing upward around the fuel rods, resulting in an outlet temperature 5K higher than the pseudo-critical temperature of 557.7K at a pressure of 25MPa. An inner steam plenum above the core eliminates hot streaks. The second pass, called "superheater", with a downward flow, heats the coolant up to 706K. After a second mixing in an outer mixing plenum below the core, the coolant is finally heated up to 803K with an upward flow in a second superheater located at the core periphery, known as the third pass. Each pass, the evaporator and both superheaters, is built of 52 fuel assembly clusters as shown in **Fig. 3.2** (Schulenberg and Starflinger, 2007). Therefore the complete reactor core is composed of 156 assembly clusters.

The 7×7 square arrangement design proposed by Hofmeister et al. (2007) of 40 fuel rods with an 8mm outer diameter distributed in dual rows and a single water tube replacing 9 fuel rods was used. The fuel rods and the water tube are housed within an assembly box and are grouped into a cluster of 9 assemblies, with a 3×3 arrangement. A common head and foot piece, of similar in dimensions to the head in PRWs, is used to ease the handling of the assembly boxes during revisions, and this permits a reduction of the number of individual control rod drivers.

The control rods are inserted from the core top into 5 of the 9 water tubes of a cluster (**Fig. 3.2**). The structural material for cladding, assembly boxes and water tubes is stainless steel. The main reactor parameters are presented in **Table 3.1**.

Table 3.1. Main reactor parameters (Schulenberg and Starflinger, 2007).

Reactor parameter	Reference value
Thermal power	2000 MWt
Efficiency	44%
Pressure	25 MPa
Coolant inlet core temperature	553 ºK
Coolant outlet core temperature	800 ºK
Coolant inlet mass flow*	1200 kg/s
Fuel material**	UO_2
Cladding material	Stainless steal
Total number of fuel rods in the core	56160

* Reiss et al. (2008).

** Uranium enrichment of 5% for all fuel rods except the corner rod which is enriched to 4%.

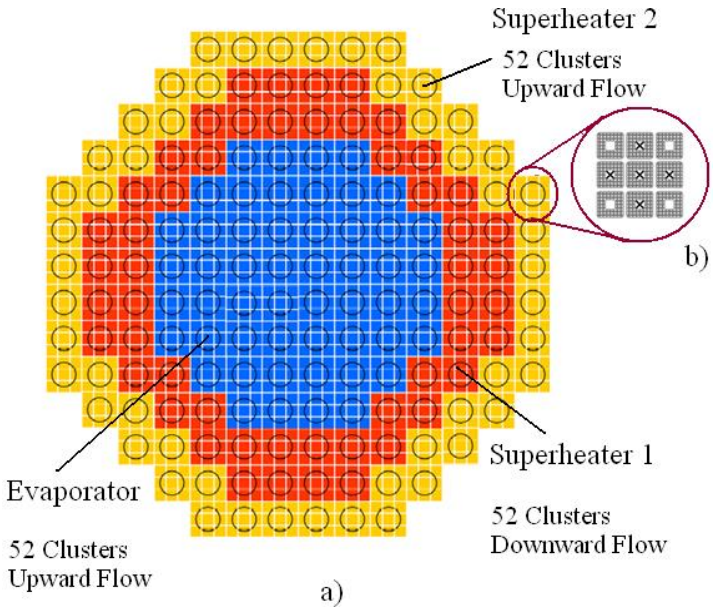

Figure 3.2. a) Arrangement of evaporator and superheaters 1 and 2; **b)** assembly cluster with water tubes and control rods (Starflinger et al., 2010).

3.2. Conceptual Model

The core consists of three vertically oriented circular tubes. In the first and third step (Channels 1 and 3) the coolant flows upward, while in the second step (Channel 2) the coolant flows downward (**Fig. 3.3**); each channel is divided into 21 axial nodes.

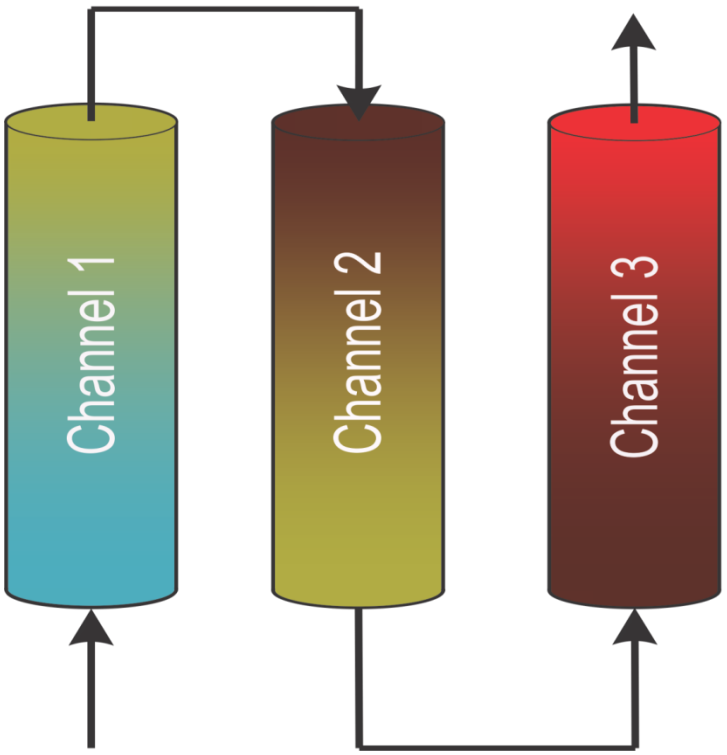

Figure 3.3. Arrangement of the computational nodes in the core model.

In the heated channels with supercritical fluids, a sudden change in fluid density exists. No phase change occurs during the heat-up process, hence, the heat transfer analysis takes into account a single supercritical phase.

The understanding of the thermal-hydraulic behavior of rod bundles requires determining the flow condition in sub-channels due to the changes presented in the fluid properties of the fuel assembly.

3.3. Physical Properties of Super-Critical Water

The thermal physical properties at supercritical pressure used in this work were taken from Wagner and Kretzschmar (2008). In **Fig. 3.4** the behavior of these properties at 25 MPa are shown. It is important to note that in the range of temperatures between 350 to 450 °C the changes in all the parameters are significant.

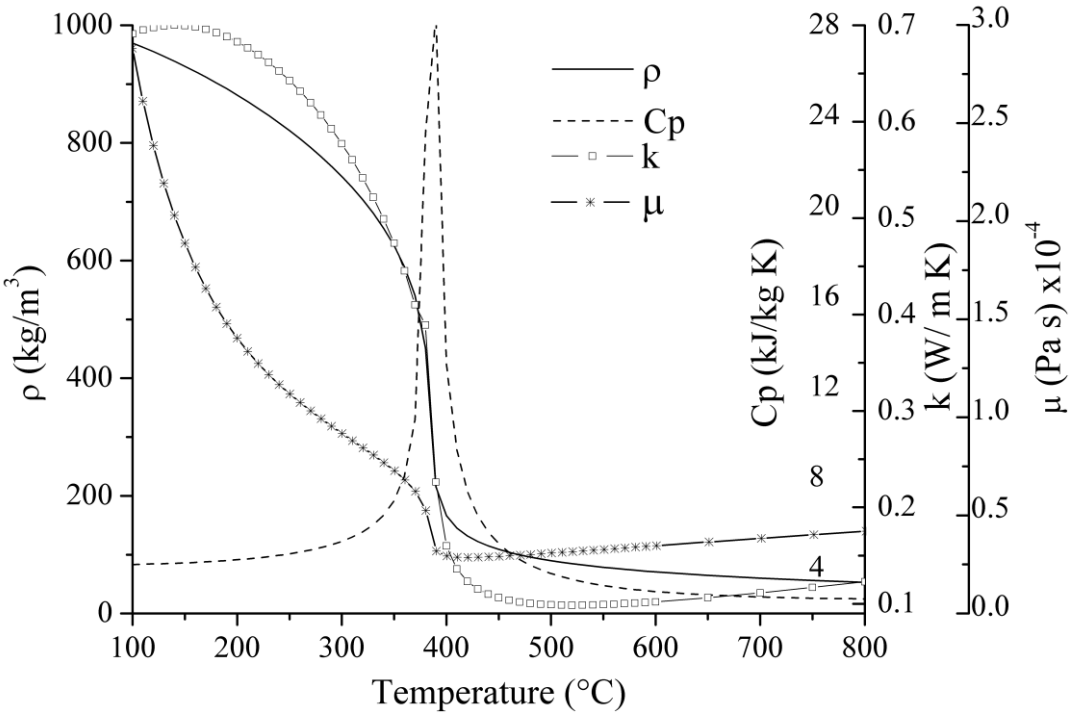

Figure. 3.4. Behavior of specific heat (Cp), thermal conductivity (k), viscosity (μ) and density (ρ), as functions of water temperature at 25 MPa.

CHAPTER IV

NUMERICAL EXPERIMENTS

4.1. Numerical Analysis of Heat Transfer Correlations

The supercritical water heat transfer correlations applied in this work are shown in **Table 4.1**. Dimensionless numbers are given by Eq. (2.6).

McAdams (1942) proposed the use of the Dittus-Boelter correlation for forced-convective heat transfer in turbulent flows at subcritical pressures. The only difference between the Dittus-Boelter and McAdams correlations is that the latter has a larger coefficient. According to Schnurr et al. (1976), it agrees with experimental data. However, it was noted that the correlation might produce unrealistic temperature results near the critical and pseudocritical points, due to it being very sensitive to variations in the thermal-physical properties

Bishop et al. (1964) conducted experiments in supercritical water flowing upward inside bare tubes and annuli, within the following range of operating parameters: P=22.8–27.6 MPa, Tb=282–527ºC, m=651–3662 kg/m^{2}s and q=0.31–3.46 MW/m^2. Their data for heat transfer in tubes were generalized with a fit of ±15%. This correlation uses a cross-sectional averaged Prandtl number and the final term in the correlation (1+2.4 D/x) accounts for the entrance-region effect. Bishop et al.'s correlation was modified and used without the entrance-region term, because this term depends significantly on the particular design of the inlet of the bare test section.

Table 4.1. Supercritical Water Heat-Transfer Correlations (HTCs).

Correlation	Reference
$Nu_b = 0.023 Re_b^{0.8} Pr_b^{0.4}$	Dittus and Boelter (1930)
$Nu_b = 0.0243 Re_b^{0.8} Pr_b^{0.4}$	McAdams (1942)
$Nu_b = 0.0069 Re_b^{0.9} \langle Pr_b \rangle^{0.66} \left(\frac{r_w}{r_b}\right)^{0.43} \left(1 + 2.4\frac{D}{x}\right)$	*Bishop et al. (1964) with ERE
$Nu_b = 0.0069 Re_b^{0.9} \langle Pr_b \rangle^{0.66} \left(\frac{\rho_w}{\rho_b}\right)^{0.43}$	*Bishop et al. (1964) without ERE
$Nu_w = 0.00459 Re_w^{0.923} \langle Pr_w \rangle^{0.613} \left(\frac{\rho_w}{\rho_b}\right)^{0.231}$	Swenson (1965)
$Nu_b = 0.0053 Re_b^{0.914} \langle Pr_b \rangle^{0.654} \left(\frac{\rho_w}{\rho_b}\right)^{0.518}$	Mokry et al. (2009) preliminary
$Nu_b = 0.0061 Re_b^{0.904} \langle Pr_b \rangle^{0.684} \left(\frac{\rho_w}{\rho_b}\right)^{0.564}$	Mokry et al. (2009) final

* with Entrance-Region Effects (ERE) and a fit of ±15%; $\langle Pr \rangle$ is the average; *b* and *w* means bulk-fluid and *w*all temperature, respectively.

Swenson et al. (1965) have suggested a correlation in which thermal-physical properties are mainly based on a wall temperature, as they found that conventional correlations, which use a bulk-fluid temperature as a basis for calculating the majority of thermal-physical properties, did not work as well.

A dimensional analysis was performed by Mokry et al. (2009) in order to obtain a general empirical form of correlation for the heat transfer calculations, and as a result of the experimental data analysis, two correlations for the heat transfer coefficient at supercritical water conditions were obtained.

In **Fig. 4.1** the results for Channel 1 are presented, showing the Wall Temperature behavior for different correlations presented in Table 1. It should be noted that the last node temperature (at 4 m) is practically the same, and the trend is very similar for all the correlations, except for a short zone where the Swenson correlation yields a lower temperature while Mokry's correlations (both preliminary and final) yield a higher temperature, the same was noted for the Bishop's correlations (with and without ERE).

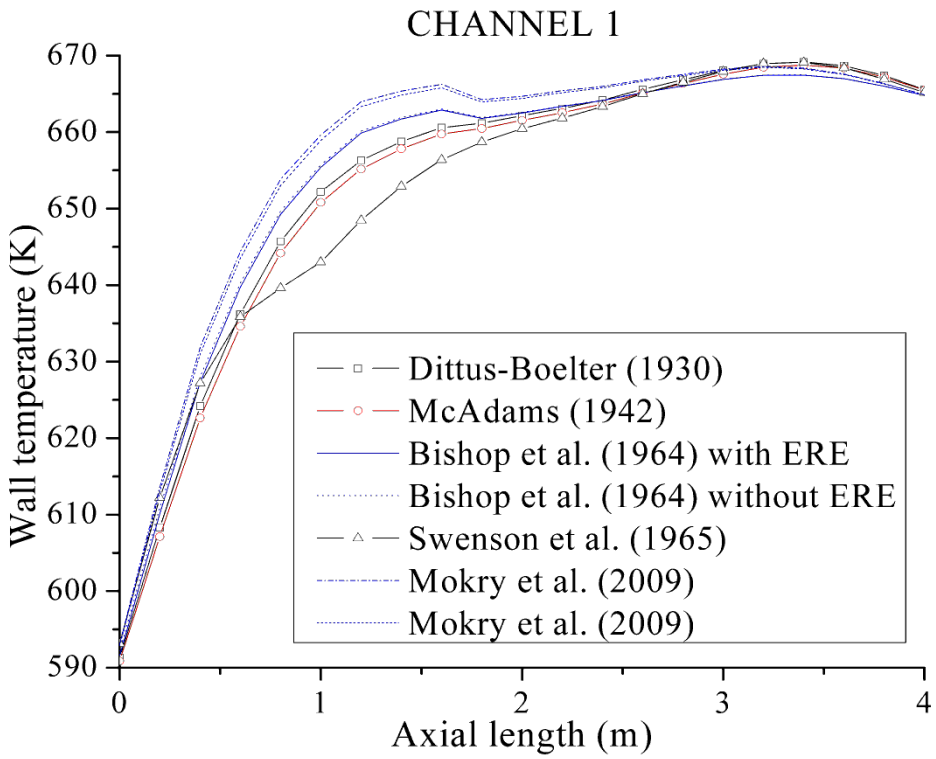

Figure. 4.1. Simulation results for Channel 1 showing the wall temperature behavior for different HTCs.

In **Fig. 4.2** the results for Channel 2 are presented, showing the wall temperature behavior for the correlations in **Table 4.1**. Similar results were obtained, however contrary to what was

observed in Channel 1, the Swenson's correlation yields slightly higher temperatures along the entire channel meanwhile the Bishop's (with and without ERE) and Mokry's correlations yield slightly lower temperatures along the entire channel.

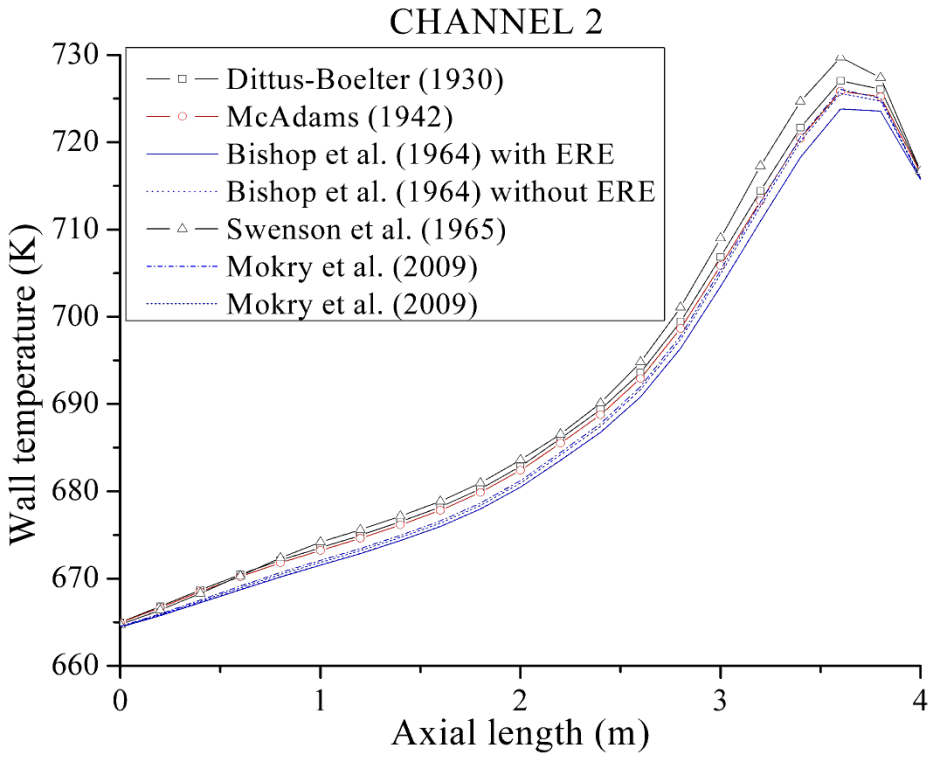

Figure. 4.2. Simulation results for Channel 2 showing the wall temperature behavior for different HTCs.

Fig. 4.3 presents the results for Channel 3, showing the wall temperature behavior for the correlations presented in **Table 4.1.** In this case, the trends that most resemble each other are presented. Again, the Swenson's correlation deviates the most, yielding slightly higher temperatures than other correlations.

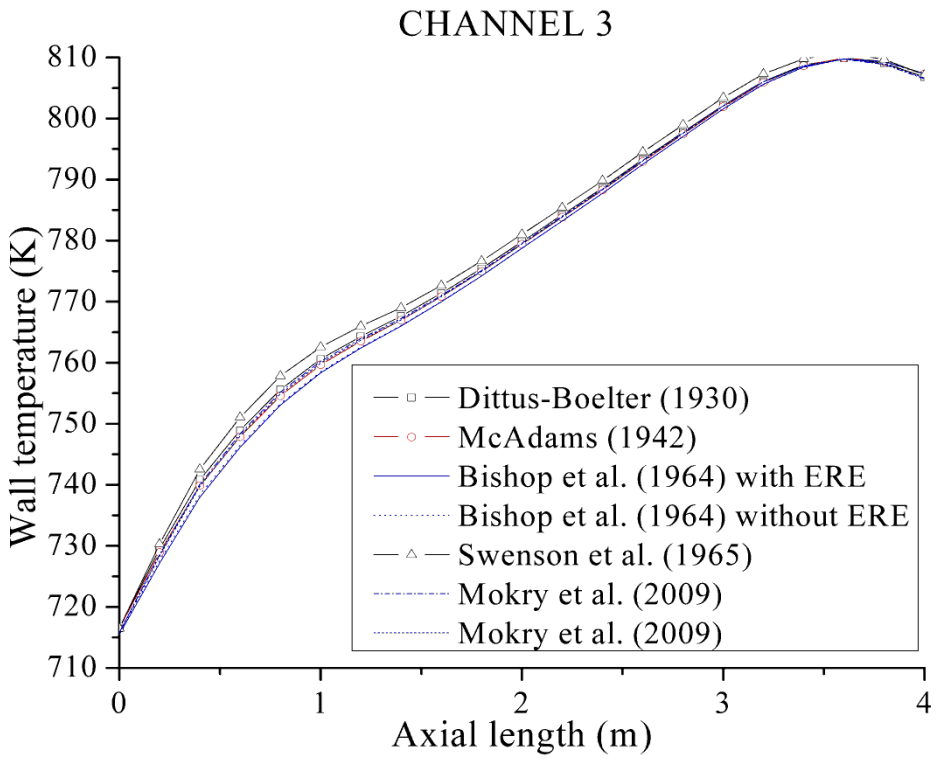

Figure. 4.3. Simulation results for Channel 3 showing the Wall Temperature behavior for different HTCs.

In **Fig.4.4** the results along the three channels are presented. It should be noted that Swenson's correlation is the one with greater deviation from Dittus-Boelter's correlation, with a difference of 10K in Channel 1.

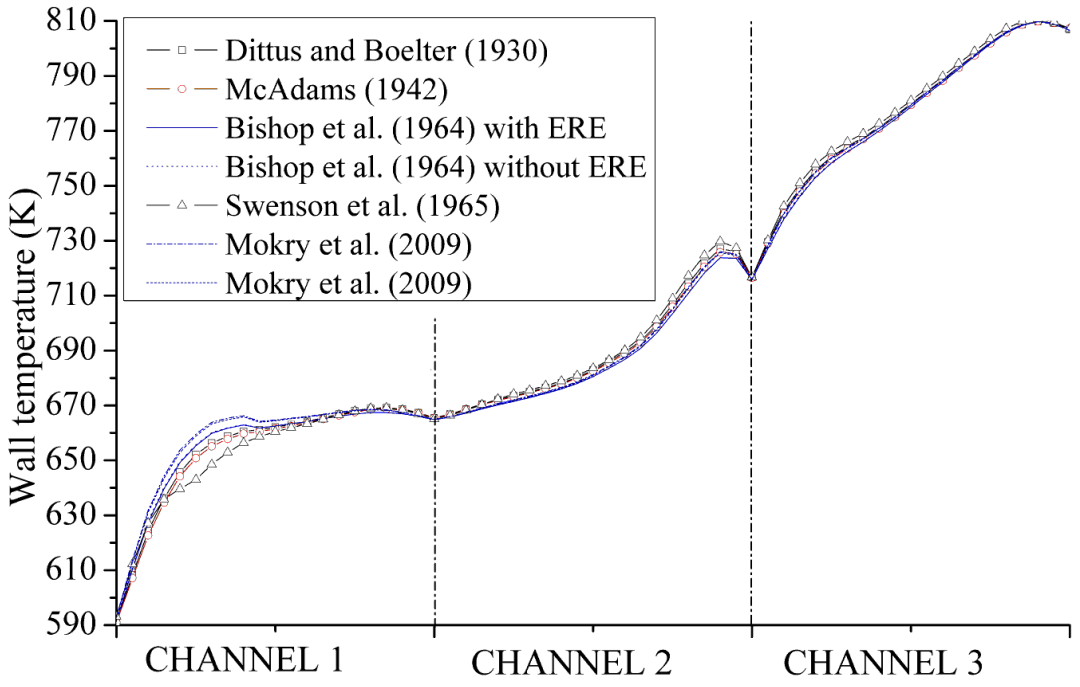

Figure. 4.4. Simulation results showing the wall temperature behavior across the three channels for different HTCs.

There is a wall temperature reduction at the end of each channel; especially for Channel 2, and this is due to the axial distribution of thermal power which has a minimum in this bottom core zone. This is an undesired result of the three pass core concept.

An important finding in this numerical analysis is that Swenson's correlation gave the most conservative predictions, in terms of safety, because higher temperatures are calculated due to the use of the wall temperature for the Re and Pr calculations, while other correlations use the bulk temperature.

4.2. Steady State Analysis

The aim of the steady state analysis, without temperature feedback effects (reactivity effects), was to predict the effect of the fluid's physical properties close to the supercritical and critical pressures in the behavior of the reactor core under those conditions.

Twenty one numerical experiments were executed to predict the temperature distribution of the cooling in each channel for different values, from 1100 to 1300 kg/s, of mass flux in the inlet of the core.

The numerical results are presented in **Figs. 4.5-4.10**. **Fig. 4.5** shows the behavior of the HTC along the length of the core for the three channels. This experiment was executed for a mass flux of $621.6\ \mathrm{kg/m^2K}$ and a pressure of $25\ \mathrm{MPa}$. In Channel 1, the HTC exhibits a sharp increase of $25{,}000\ \mathrm{W/m^2K}$ to $44{,}000\ \mathrm{W/m^2K}$ with a value of $15{,}000\ \mathrm{W/m^2K}$ at the end. The behavior of the HTC, at supercritical pressure, is primarily characterized by the thermal physical properties which vary markedly, especially near the pseudo-critical condition as illustrated in **Fig.3.4**.

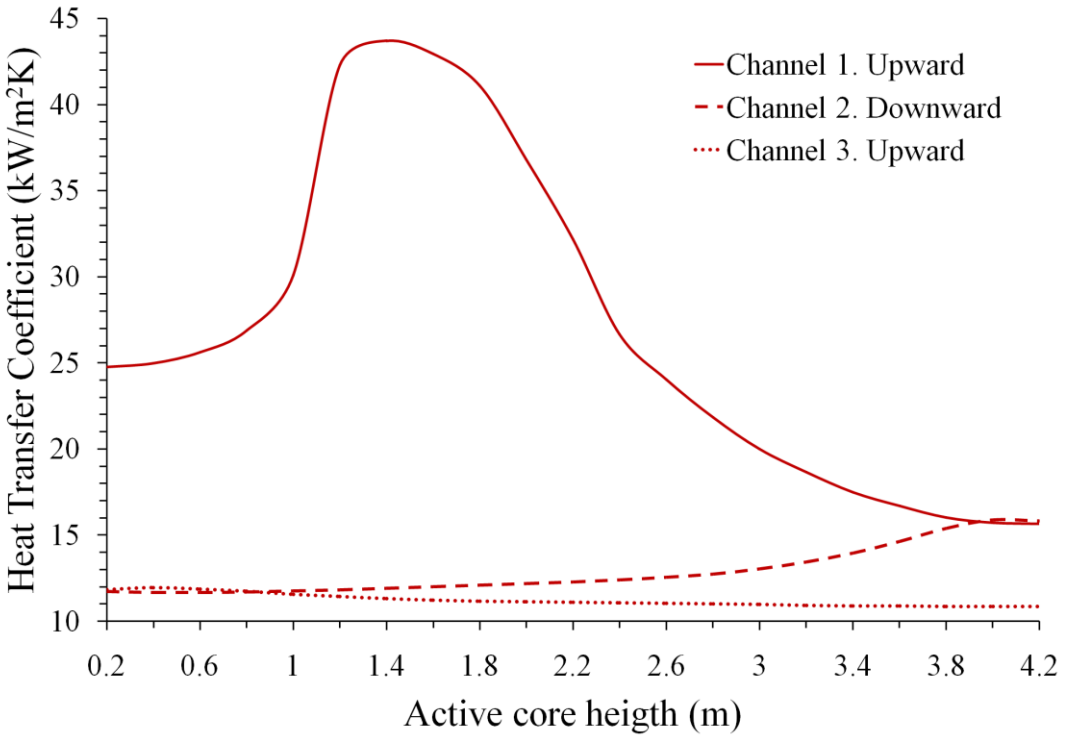

Figure 4.5. HTC behavior at constant pressure with a mass flux of 621.6 kg/m^{2}s in the three channels: the evaporator, and the superheaters 1 and 2 are represented for Channel 1, Channel 2 and Channel 3, respectively,

Figs. 4.6-4.9 show the temperature axial profiles for the fuel peak, gap, wall-cladding and coolant for a mass flux of 1200 kg/s in the core. **Fig. 4.6** shows the peak temperature profile in the fuel, whose magnitude is a function of the axial power distribution in each channel. **Fig. 4.7** shows the axial temperature profile in the gap; a large temperature decrease from the fuel temperature was observed, as expected, however both temperatures follow similar trends. **Fig. 4.8** and **Fig. 4.9** show the temperature profiles in the wall and coolant through the axial channel. A significant temperature increase at each step of the core was observed. In the case of the wall temperature distribution (**Fig. 4.8**), in Channel 1, the temperature increase was 74.4K, with an inlet temperature of 591.3K and an outlet temperature of 665.7K; in Channel 2, the temperature increased by 52.1K, with an outlet temperature of 717.8K ; and in Channel 3, the temperature

increased by 94K, where the outlet temperature was 811.8K. The coolant temperature increase (**Fig. 4.9**) in Channel 1 was 77.5K, with an inlet temperature of 586K; the temperature increase in channels 2 and 3 was 48.9K and 94.6K, respectively, with an outlet temperature of 807K in Channel 3. The concept of the three channels in the core, their flow trajectories and multiple heat-up steps enhance the heat transfer process and consequently the thermal efficiency of the SCWR.

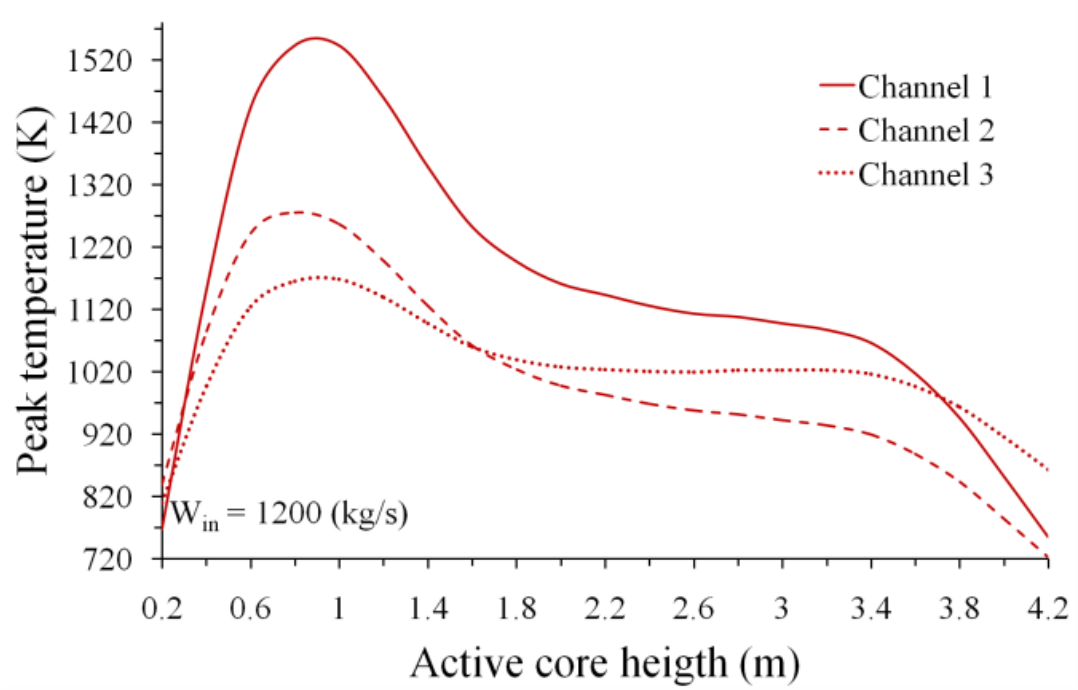

Figure 4.6. Axial temperature distributions of fuel peak for a mass flux of 1200 kg/s in the core.

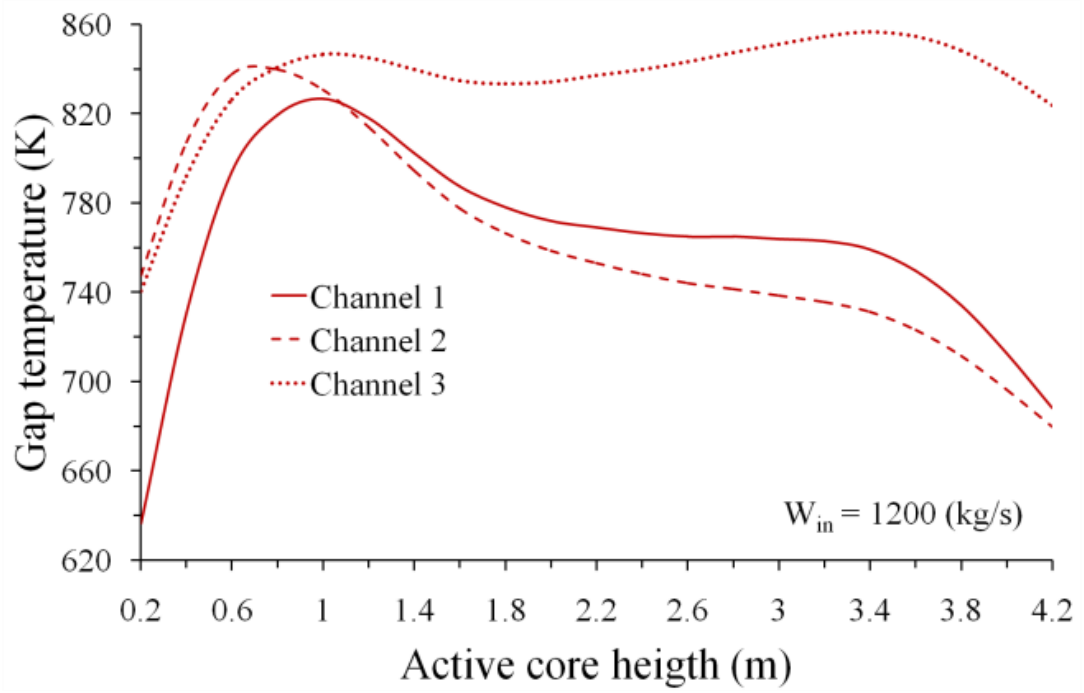

Figure 4.7. Axial temperature distributions of gap for a mass flux of 1200 kg/s in the core.

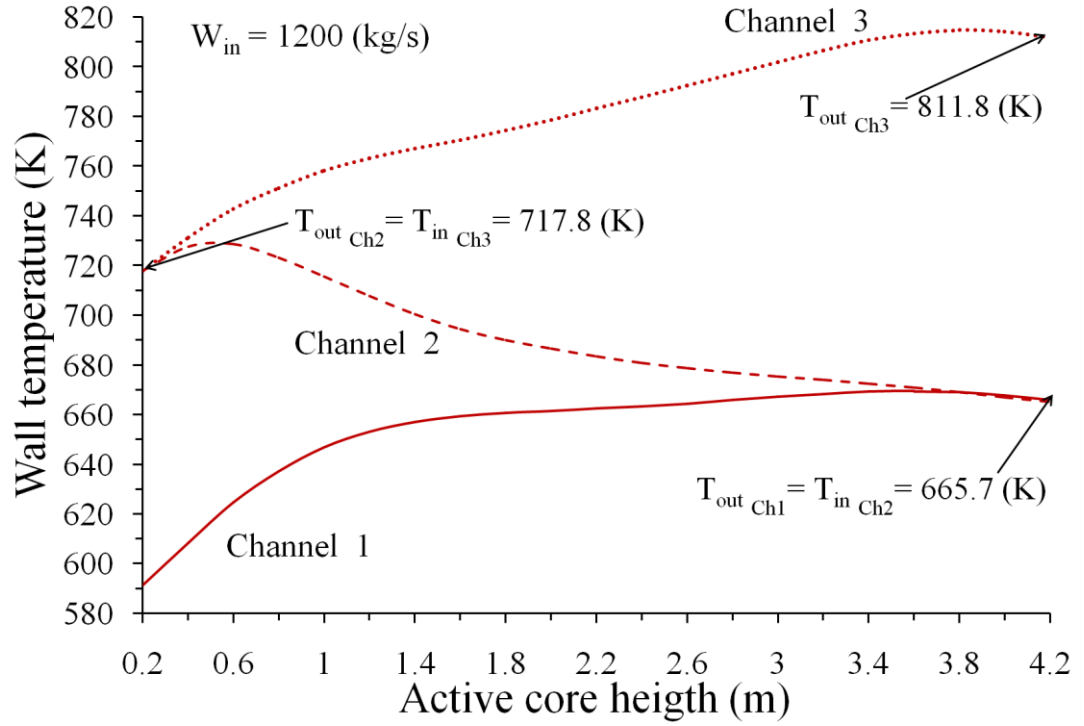

Figure 4.8. Axial temperature distributions of wall cladding for a mass flux of 1200 kg/s in the core.

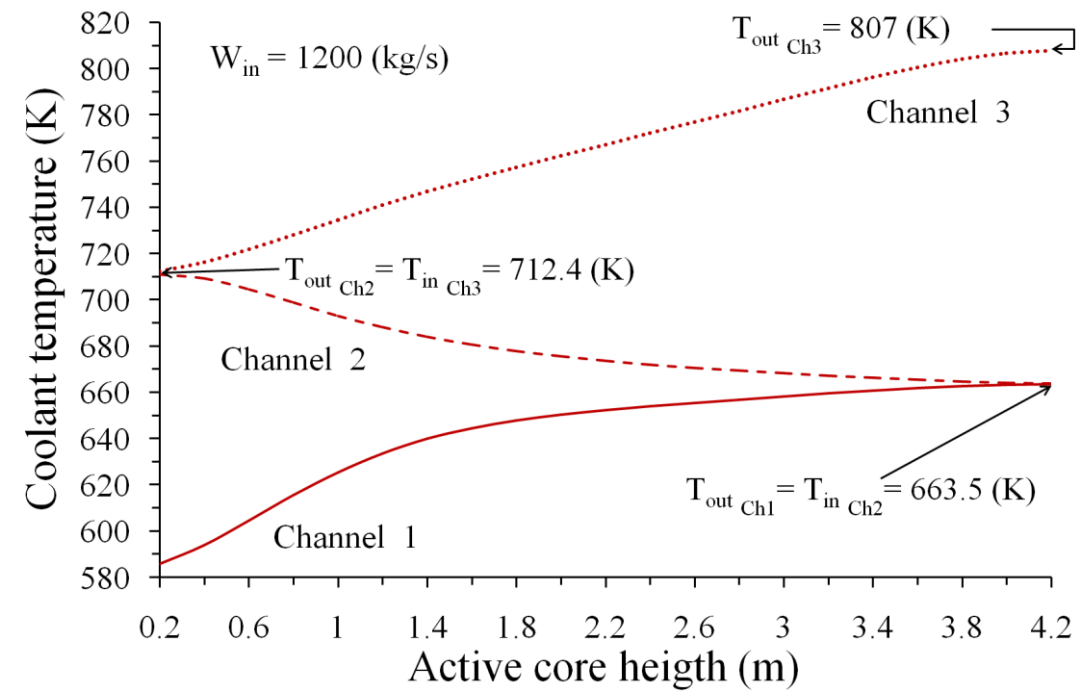

Figure 4.9. Axial temperature distributions of coolant for a mass flux of 1200 kg/s in the core.

Numerical analyses were applied for different mass flux values of coolant (W_{in}) in the core within the range of 1,100 to 1,300 kg/s. Results of temperature profiles of the coolant are shown in **Fig 4.10**. The heat transfer is improved while the mass flow in the core increases, the numerical results indicate that the coolant temperature increase, at each step is greater for 1,100 kg/s than for 1,200 and 1,300 kg/s. This produces a relatively significant increase in the coolant temperature in Channel 3.

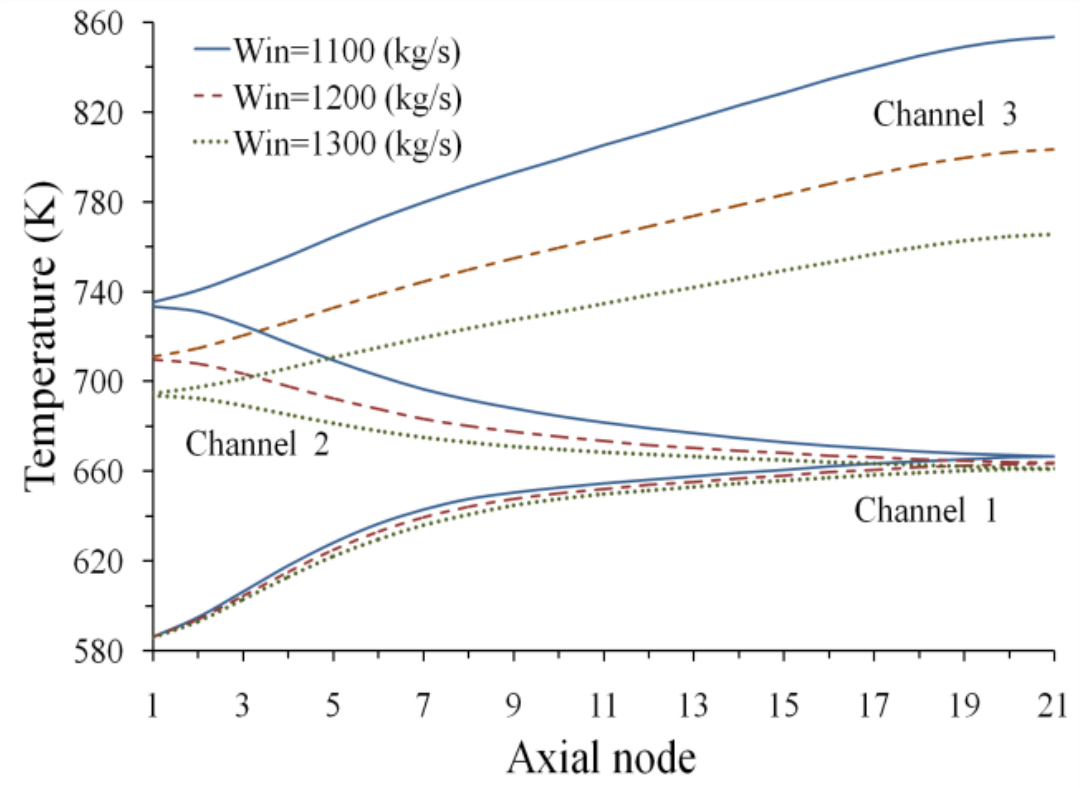

Figure 4.10. Coolant temperature axial distribution for different inlet mass fluxes in the three channels.

4.3. Transient Analysis with Temperature Feedback Effects

The reactor power is given by,

$$P(t,z) = n(t)F(z)P_0 \tag{4.1}$$

where $F(z)$ is the axial power factor, P_0 is the nominal power and $n(t)$ is the normalized neutron density, which is calculated from a point reactor kinetics model with six groups of delayed neutrons,

$$\frac{dn(t)}{dt} = \frac{\rho(t) - \beta}{\Lambda} n(t) + \sum_{i=1}^{6} \lambda_i c_i \tag{4.2}$$

$$\frac{d\,c_i(t)}{dt} = \frac{\beta_i}{\Lambda} n(t) + \lambda_i c_i(t); \qquad i = 1,2,..,6 \tag{4.3}$$

where c_i is a delayed neutron concentration of the *i*th precursor group normalized with the steady-state neutron density, ρ is the net reactivity, β is the neutron delay fraction, Λ is the neutron generation time and β_i is the portion of neutrons generated by the *i*th precursor group. The initial conditions are given by $n(0) = n_0$ and $c_i(0) = \beta_i n_0 / \Lambda\lambda_i$. The parameters of the kinetics model are presented in Table 2.

Table 4.2. Kinetics parameters used in the reactor power model (Duderstadt, 1976).

Group	β_i	$\lambda_i (s^{-1})$
1	2.470×10^{-4}	0.0127
2	1.355×10^{-3}	0.0317
3	1.222×10^{-3}	0.1150
4	2.646×10^{-3}	0.3110
5	8.320×10^{-4}	1.4000
6	1.690×10^{-4}	3.8700

* $\beta = 6.5 \times 10^{-3}$ *and* $\Lambda = 4.0 \times 10^{-5}$ s

The reactivity coefficient due to variations on fuel temperature was studied for the square fuel assembly design proposed by Barragán-Martínez et al. (2013). The calculations were done for the fuel assembly model along the active core height. Due to the strong variation of

coolant density through the core, five densities: 0.74, 0.45, 0.31, 0.17 and 0.09 g/cm^3 were considered. This safety parameter is calculated in order to evaluate the variation of the reactivity due to the Doppler Effect, as a function of the fuel temperature, which is related to the resonances broadening when the fuel temperature increases. The values of the reactivity as a function of the coolant density and fuel temperature are presented in **Fig. 4.11**. The values of the infinite multiplication factor obtained with HELIOS-2 for 177 energy groups were used to obtain the reactivity (Duderstadt and Hamilton, 1976).

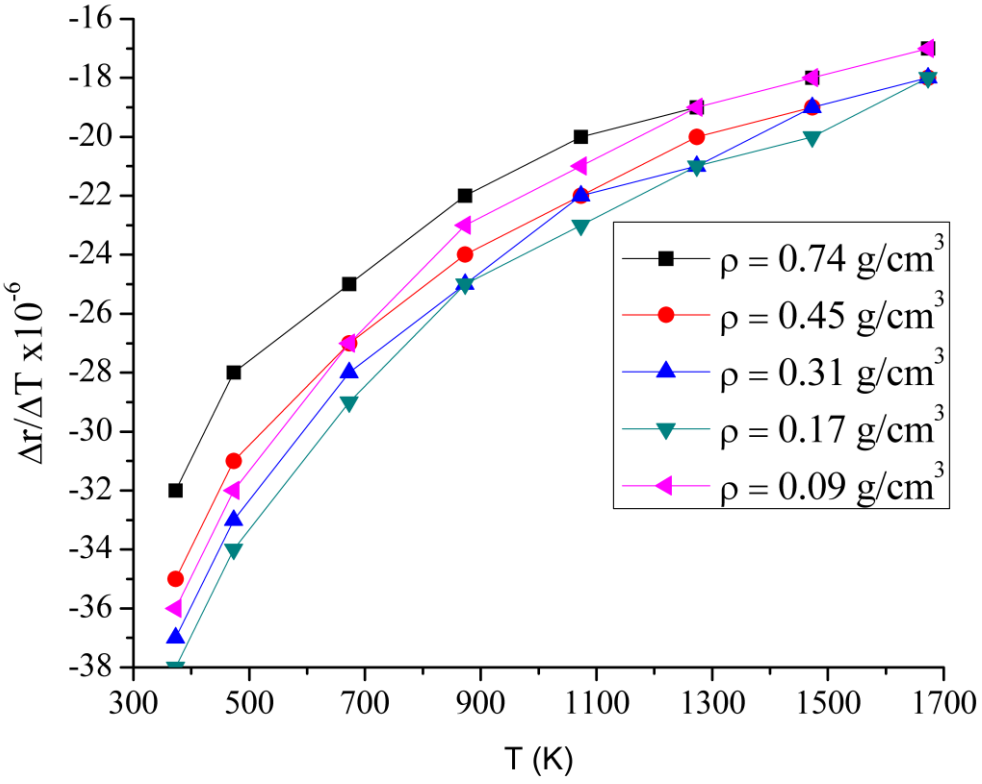

Fig. 4.11. Reactivity coefficients obtained with HELIOS-2 for 177 energy groups at different coolant densities.

The core thermal-hydraulics behavior was analyzed for the steady state and for two transients applying models with temperature feedback effects. The core transient behavior has been

analyzed during a flow reduction from 100% to 90%, and 60% (**Fig. 4.12**), only extensive results for 60% reduction are presented in **Figs. 4.13-4.15**.

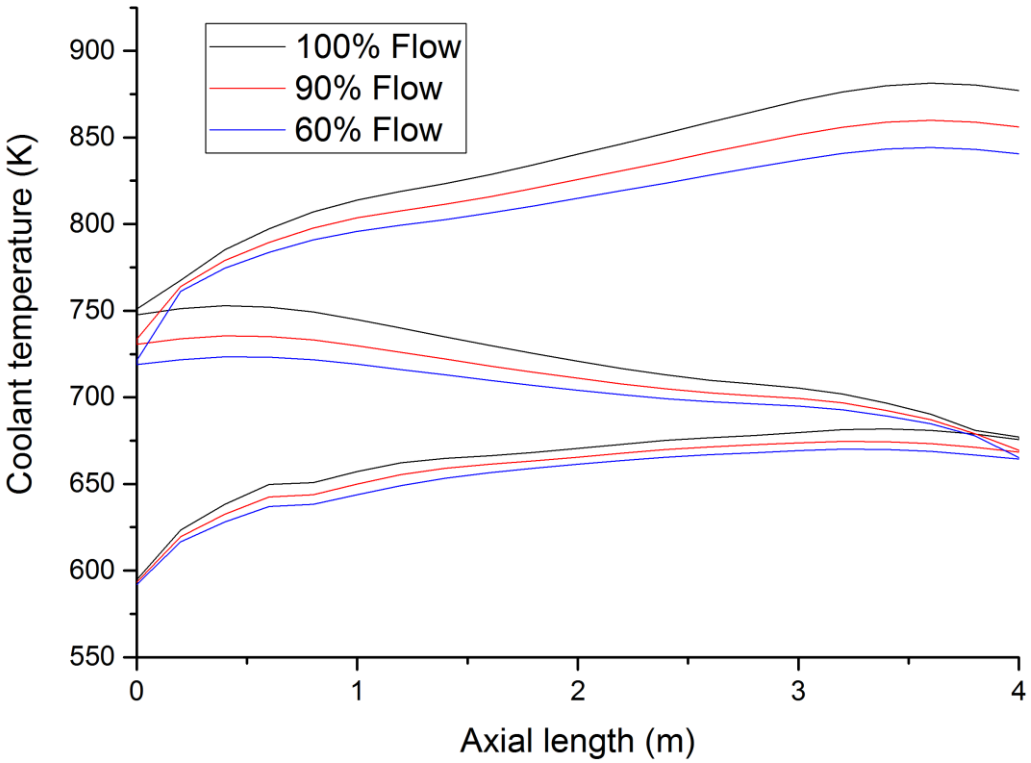

Figure 4.12. Coolant temperature for different inlet flows.

In order to avoid hot spots the core needs to be redesigned, as initially proposed by Hofmeister et al. (2007), and Schulenberg and Starflinger (2007). A recent work of Wank et al. (2010) analyzed and discussed the proposed core design of Schulenberg and Starflinger (2007), where two chambers were added between the heat-up regions. Inside the two chambers the cooling water is mixed.

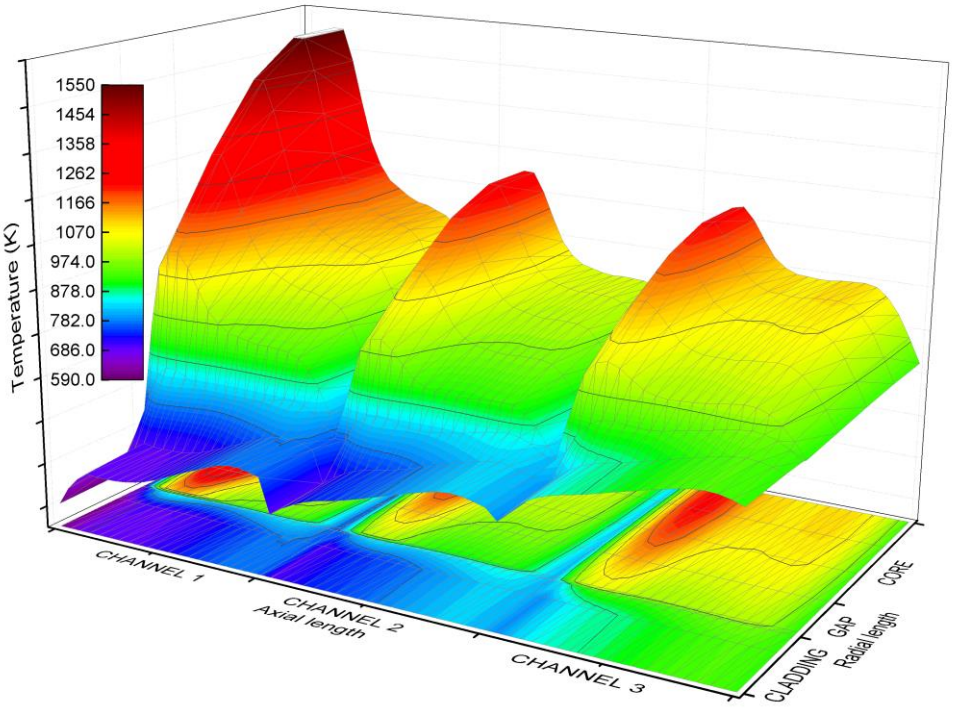

Figure 4.13a. Average temperature distribution in the axial and radial nodes for the three channels at the beginning (t=0 s) of flow reduction of 60% transient.

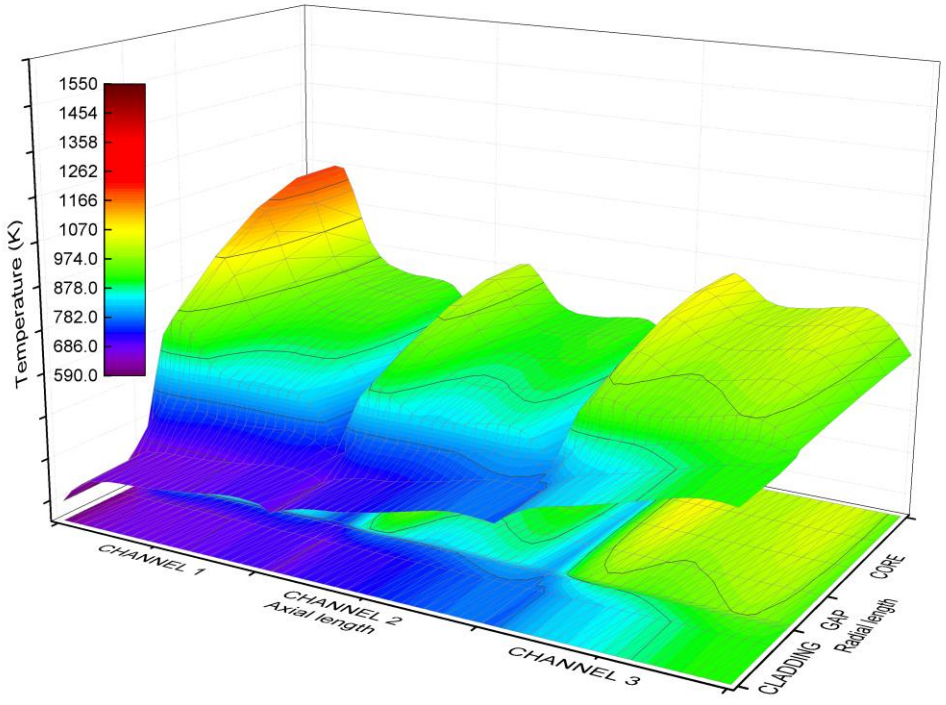

Figure 4.13b. Average temperature distribution in the axial and radial nodes for the three channels at the middle (t=20 s) of flow reduction of 60% transient.

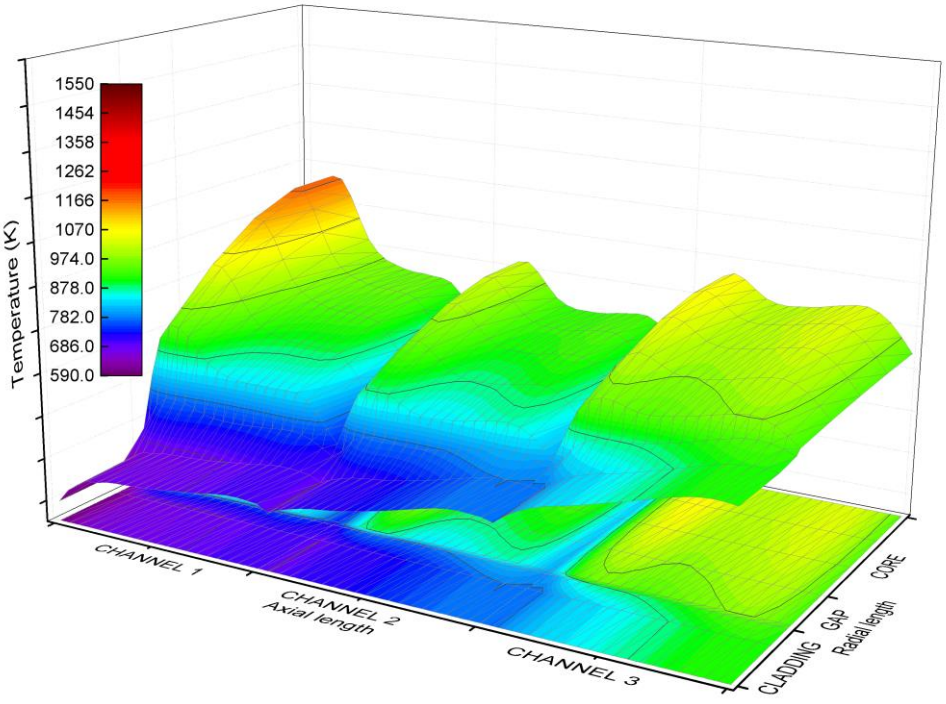

Figure 4.13c. Average temperature distribution in the axial and radial nodes for the three channels at the end (t=40 s) of flow reduction of 60% transient.

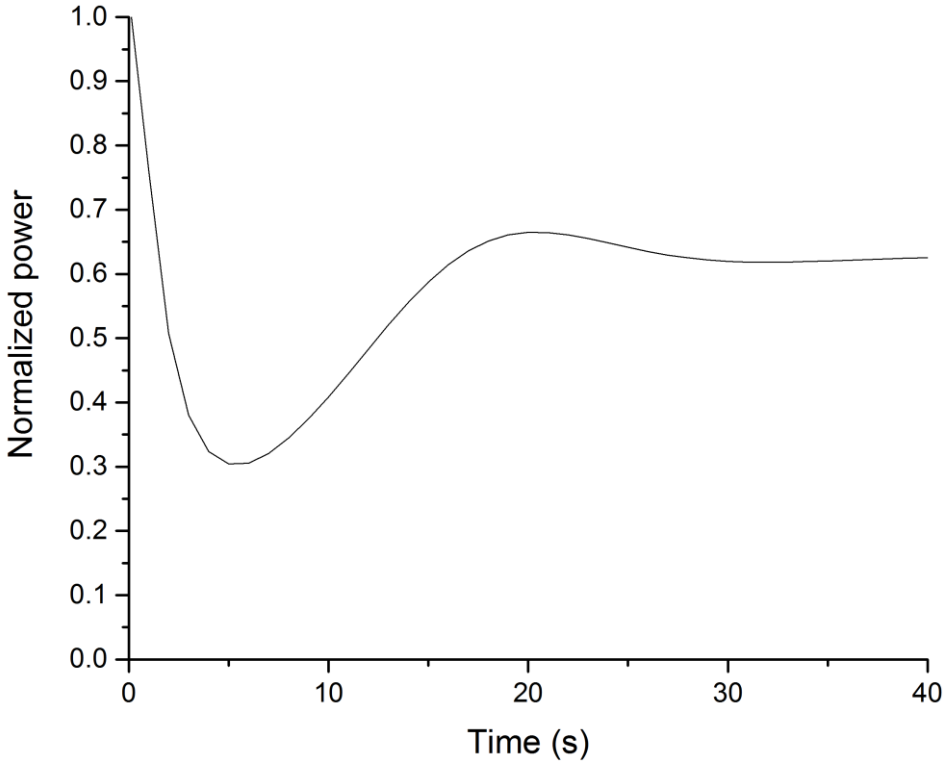

Figure 4.14. Power behavior for a flow reduction of 60% transient.

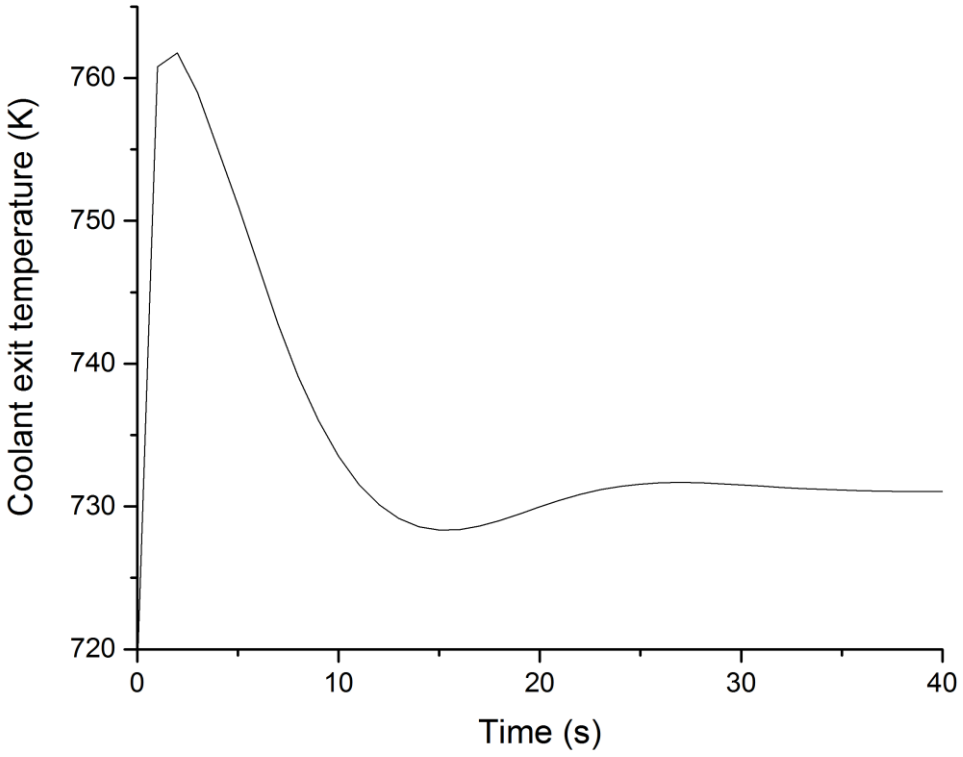

Figure 4.15. Coolant exit temperature behavior for a flow reduction of 60% transient.

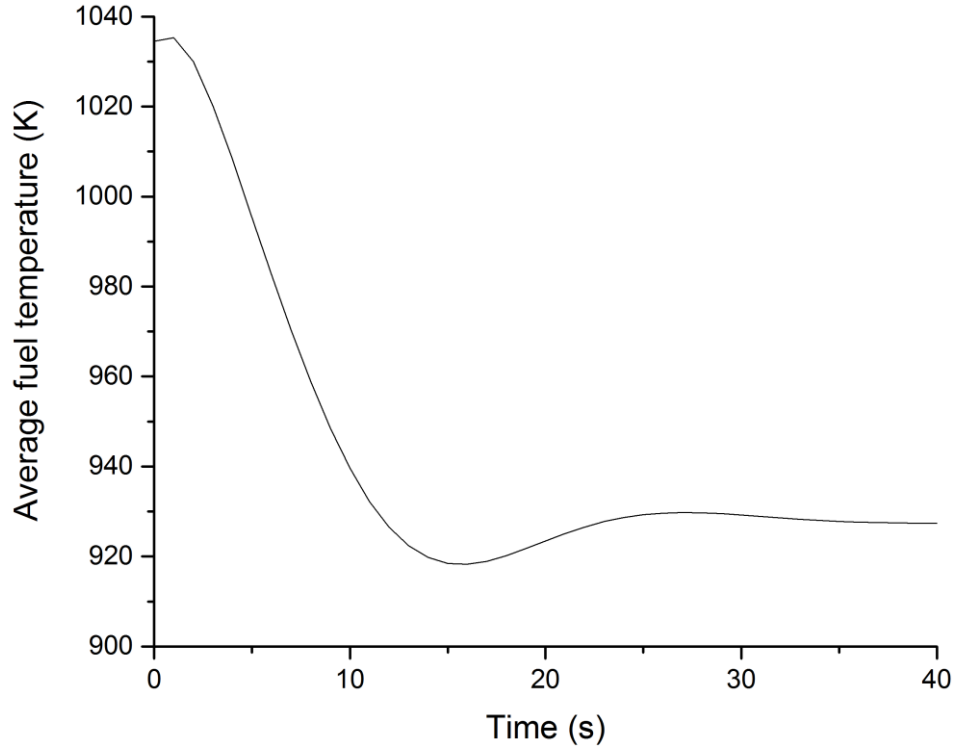

Figure 4.16. Average fuel temperature behavior for a flow reduction of 60% transient.

4.4. MonteCarlo Simulations

To obtain mathematical expressions, i.e., a sensitivity analysis, which describes the behavior of SCWR power, fuel temperature and total reactivity depending on core inlet flow, a Monte Carlo based methodology simulation applies. Monte Carlo simulation methodology was applied systematically to establish the power operation domain with the core inlet flow system in a SCWR. This methodology is described as follows,

Step 1. Random number generation with normal distribution $N(0,1)$. It is important to use random samples with a similar distribution function as the phenomena under study.

Step 2. The numbers with normal distribution are applied to a variable, in this case core inlet flow, in order to obtain a random sample of input variable.

Step 3. The Monte Carlo method is applied in a numerical model of a SCWR reactor, in order to construct a distribution of reactor power, fuel temperature and total reactivity, i.e., obtain the output variables.

Step 4. The Monte Carlo methodology is applicable to systems at steady state, for this reason it is necessary to determine the time it takes for the system to reach a new steady state by applying the input variable to the model.

Step 5. To ensure that the output variables are independent of the simulation size, an invariability test is applied, i.e., in order to determine the size of the random sample input variables for the Monte Carlo's analysis.

Step 6. Analysis of the core inlet flow on the power reactor, fuel temperature and total reactivity behavior is performed.

Random Number Generation

To generate random numbers with normal distribution $N(0,1)$ it is required first to obtain a sample of pseudorandom numbers uniformly distributed in space. Then these numbers should be normalized to obtain a sample of pseudo random numbers uniformly distributed in the space $(0,1)$. Finally these numbers are used to generate the pseudorandom sample with normal distribution (Quezada-García et al. 2016).

Application of the Sample Random Number

The sensitivity analysis requires to obtain the output variables, i.e., a relationship between the core inlet flow as input variable and the reactor power as output variable, which is obtained by,

$$\gamma_n = \gamma_0 \left(1 + b \times N_n\right) \tag{4.4}$$

where b is the fraction in which the input variable moves, γ_0 is the value of the variable, in this case the core inlet flow, and N_n is the number n with normal distribution which was previously generated.

Applying the Monte Carlo Methodology

The input variables formed from Eq (4.1) are introduced into the conceptual model of SCWR, in order to obtain the output variables, in this case: reactor power, fuel temperature, total reactivity and inlet flow to the reactor core.

Steady State

The Monte Carlo methodology is applicable to systems at steady state. To determine the time it takes the system to reach steady state, the biggest change that the input variable can possibly have is considered, and is determined the necessary time for the SCWR to reach the steady state. Tests showed that a value of 150 seconds is required for the system to reach steady state. For this work the simulation time was, therefore, 150 seconds.

Invariability Test

The results should not depend on the size of the simulation therefore an instability analysis is applied, in this paper the Relative Standard Deviation is used,

$$RSD = \frac{s}{\bar{X}}(100) \tag{4.5}$$

where s is the standard deviation and $\bar{X}$ is the mean. The optimal value of n is obtained when the value of RSD becomes invariable with respect to the simulation size n.

Sensitivity and Uncertainty Analysis of a SCWR

Finally the output variables obtained from the input variables that describe the behavior functions that the SCWR has, depending on the core inlet flow is deducted. These functions must be adjusted to the phenomenon and contain terms of uncertainty. Confidence interval is used to understand the sensitivity of the system to changes in the core inlet flow, these were calculated using the standard formula as follows,

$$CI = \bar{X} \pm \left\{ t_{n-1} \frac{s}{\sqrt{n}} \right\} \tag{4.6}$$

Discussion

The invariability test was obtained, and for small numbers of simulations the *RSD* varies considerably. However, from 100 to more simulations, the *RSD* begins to remain constant. For simulation sizes greater than 5000 the *RSD* does not change, as shown in **Fig. 4.17**. For this study the size of the simulation is 5000, to ensure the stability of the results.

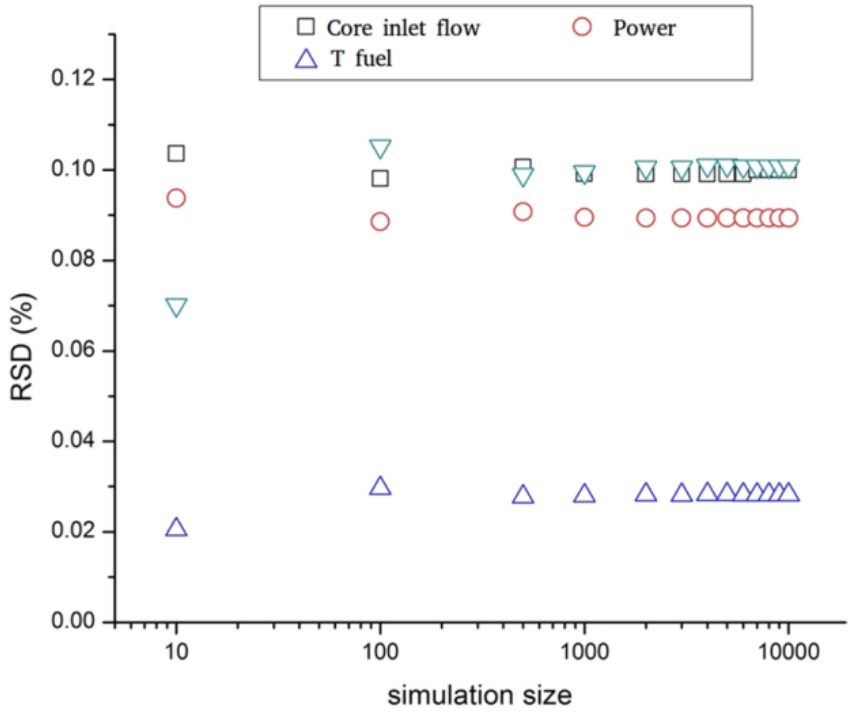

Figure 4.17. Relative standard deviation for core inlet flow, fuel temperature, reactor power and flow at the reactor core.

Then the obtained results by introducing the input variables in the conceptual model are presented. In **Fig. 4.18** the normalized reactor power is shown, and it can be observed that the reactor power is directly proportional to the core inlet flow. Also, the average temperature of the fuel is directly proportional to the core inlet flow as shown in **Fig. 4.19.** Total reactivity is also directly proportional to core inlet flow as shown in **Fig. 4.20**. Also the input stream to the first channel of the reactor core is proportional directly to the core inlet flow (**Fig. 4.21**).

Sensitivity and Uncertainty Analysis

Then the sensitivity analysis and uncertainty for each of the cases studied is presented.

Reactor Power

For the reactor power, a curve was fitted with linear regression and it was obtained a value of $R^2 = 0.9999$,

$$P_R = \left(7.18\times10^{-4} \pm 1.57\times10^{-7}\right) w + \left(0.09339 \pm 1.90\times10^{-4}\right) \tag{4.7}$$

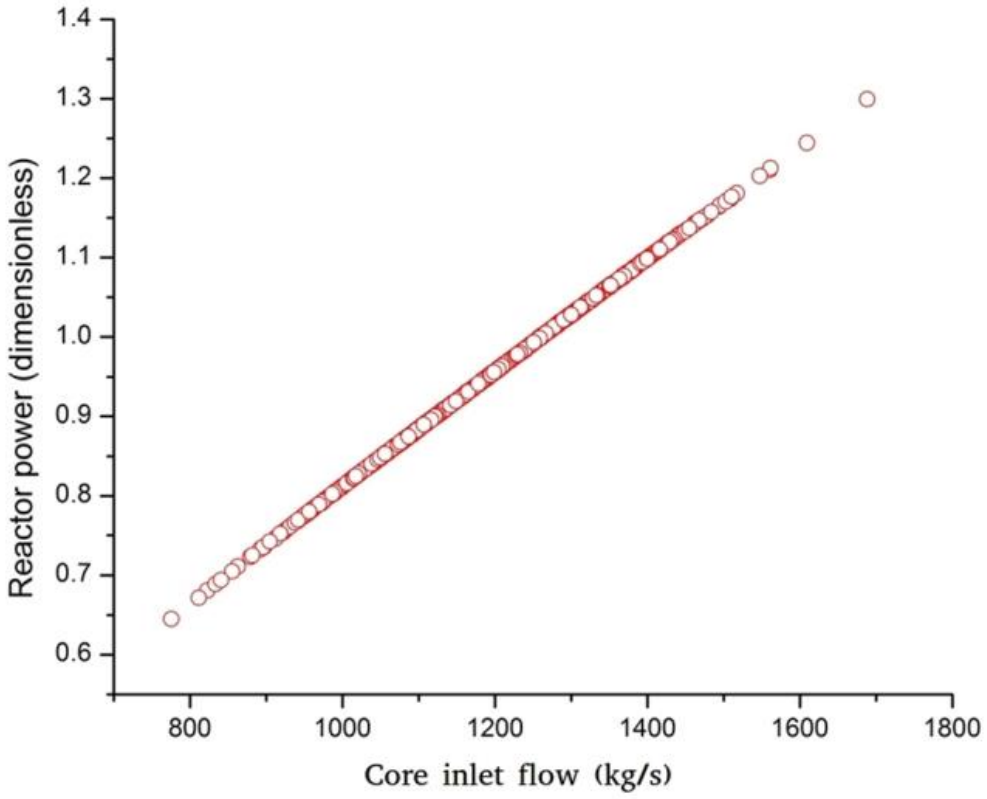

Figure 4.18. Normalized reactor power as function of core inlet flow.

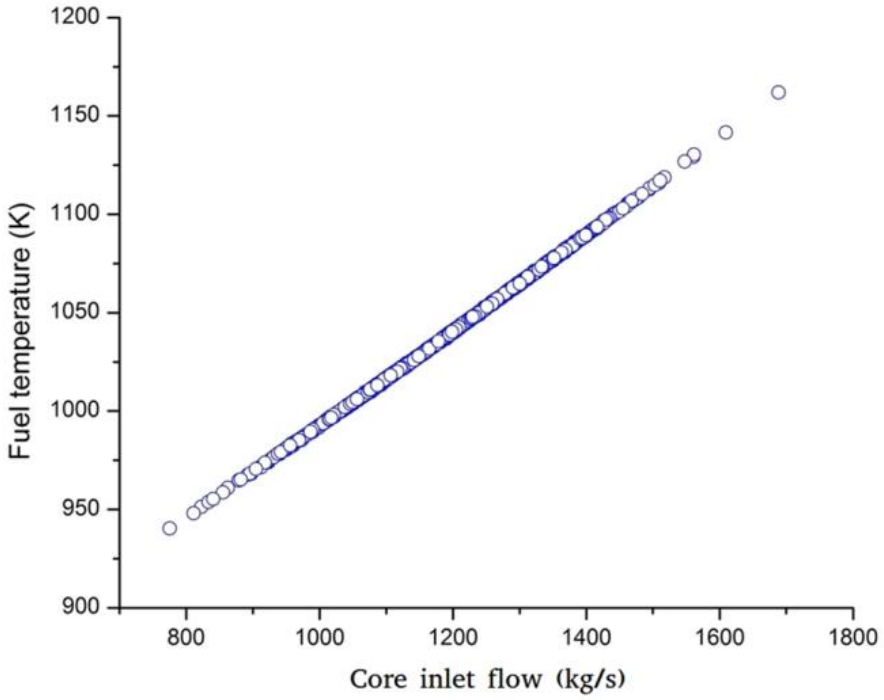

Figure 4.19. Average fuel temperature as function of core inlet flow.

Average fuel temperature

For the average fuel temperature, a curve was fitted with linear regression and it was obtained a value of $R^2 = 0.9997$,

$$T_{fuel} = \left(0.24268 \pm 9.74365 \times 10^{-5}\right)\dot{w} + \left(749.3199 \pm 0.11758\right) \tag{4.8}$$

Total reactivity

For the total reactivity, a curve was fitted with square regression and it was obtained a value of $R^2 = 0.9842$,

$$\rho_{total} = \left(-5.52688\times10^{-7} \pm 1.23346\times10^{-8}\right)\dot{w}^2 + \left(0.00204 \pm 2.96687\times10^{-5}\right)\dot{w} + \left(-1.64963 \pm 0.01776\right) \tag{4.9}$$

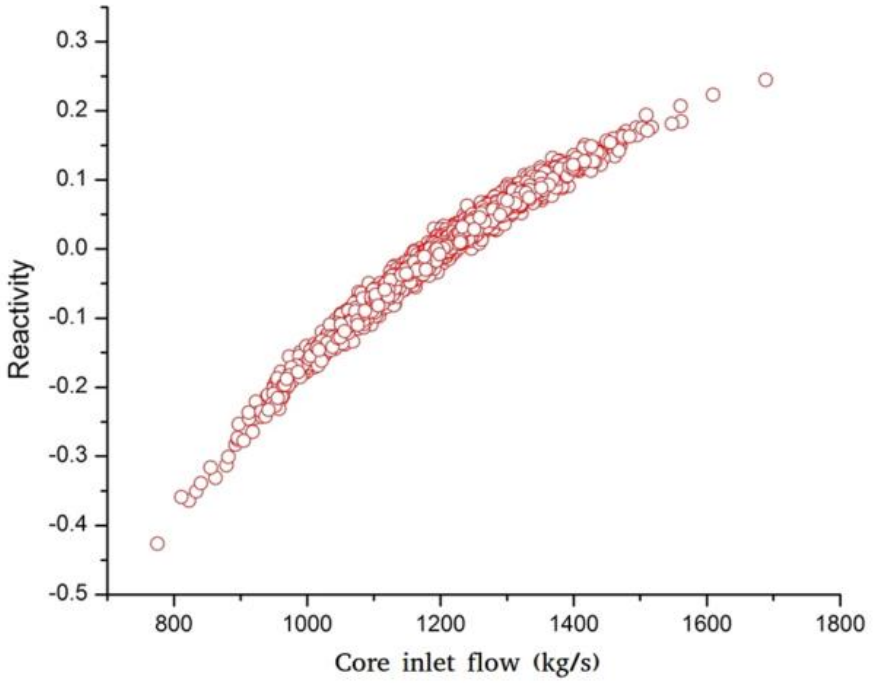

Figure 4.20. Total reactivity as a function of core inlet flow.

Inflow to the reactor core

For the inflow to the reactor core, a curve was fitted with linear regression and it was obtained a value of $R^2 = 0.9999$,

$$w_{core} = \left(5.34188\times10^{-5} \pm 5.511348\times10^{-20}\right) + \left(-2.0816\times10^{-16} \pm 4.23988\times10^{-17}\right) \tag{4.10}$$

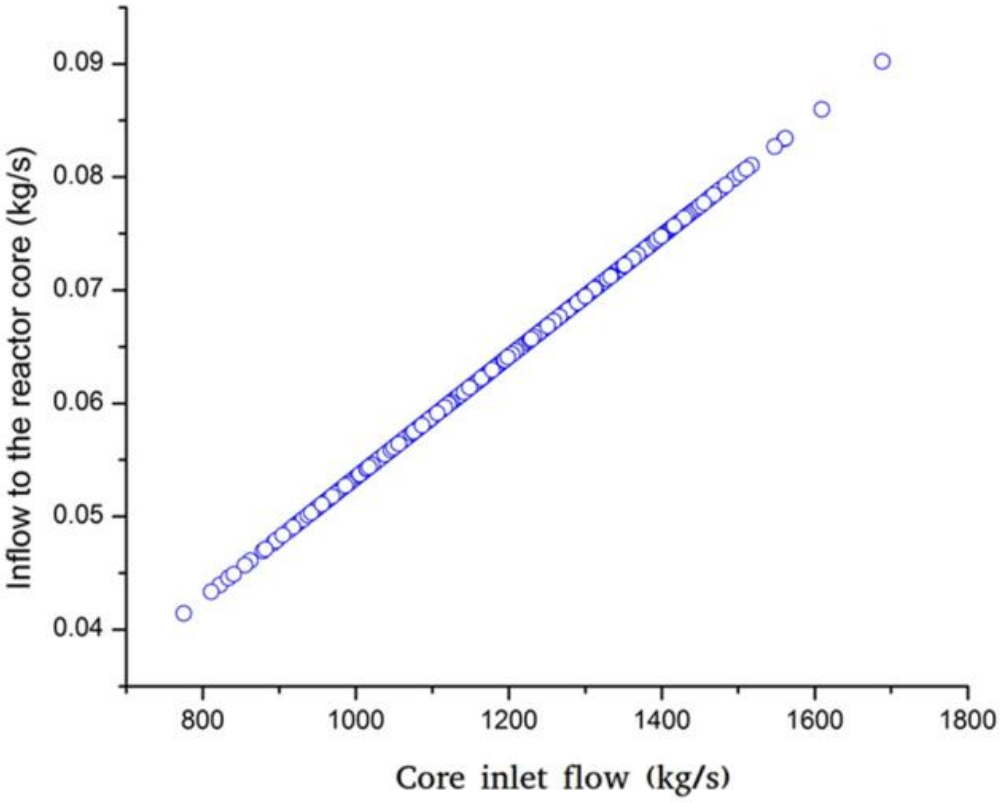

Figure 4.21. Inflow to the reactor core as a function of core inlet flow.

The results for the sensitivity analysis using a confidence interval of 95% are shown in **Table 4.3**.

Table 4.3. Sensitivity analysis confidence level (*t-student*) 95%.

Variable	Range
Core inlet flow	1195.28 - 1206.47
Reactor power	0.9524 -0.9605
Fuel temperature	1039.02 - 1042.58
Total reactivity	(-0.01024) – (-0.00235)
Core reactor inflow	0.06339 - 0.06444

CONCLUSIONS

In this Master's thesis four main objectives where performed,

1. Super-critical heat transfer correlations analysis.
2. Development of a time dependent SCWR numerical code.
3. Numerical experiments with and without temperature feedback effects.
4. Obtained equations from the Monte Carlo simulations which can predict the output variables of a SCWR as a function of core inlet flow.

Regarding the first point, the main findings are, the correlation, which agrees most with Dittus-Boelter, is McAdams. The only difference in the equation is the value of the coefficient. Bishop's correlations, with and without Entrance-Region Effect (ERE) have little differences among them in the prediction of the wall temperatures, meaning that, for this simulation the ERE is not important; predictions compared to the Dittus-Boelter correlation are a little higher in the first channel and slightly lower in channels 2 and 3. With preliminary and final Mokry´s correlations, higher temperature predictions were found in Channel 1, but were very similar to Dittus-Boelter in channels 2 and 3. Swenson's correlation showed the most deviated results, yielding lower temperatures in the first channel and higher in channels 2 and 3. Swenson's correlation uses the wall temperature for calculating the Re and Pr numbers, while the others used the bulk temperature and we found the greatest differences compared to other HTCs. For this reason Swenson's correlation could be very useful in order to find the most conservative results for Channel 3, where high wall temperatures could affect the fuel rod integrity.

Regarding the numerical experiments,

Steady State Analysis. In the three-pass core design with multiple heat-up steps the thermal-hydraulic behavior of water at supercritical conditions differs strongly from sub-critical conditions, due to a rapid variation of the thermal-physical properties in the vicinity of the pseudo-critical point. Due to the rapid change in the thermal-physical properties, a challenge is to avoid excessive hot spots of local coolant temperature and, subsequently of local cladding temperature.

For calculating the temperature axial distribution, the thermal-hydraulics calculation was applied to the three channels. The core inlet coolant temperature is set at 553K which is heated through the downcomer to 583K. Coolant density and temperature distributions in the equivalent channels and the coolant water were calculated in the axial direction of the core. The total mass flow rate is calculated to satisfy the criterion of the maximum cladding surface temperature of 893K. From this thermal-hydraulic criterion, the core outlet temperature obtained, in Channel 3 (Superheater 2), was 807K. The thermal-hydraulics calculation was carried out in the coolant, the wall, the gap and the fuel. The numerical results show that the core concept of three channels in the core and multiple heat-up steps enhance the heat transfer process, and therefore enhance the efficiency of the HPLWR.

Temperature profiles of the coolant for different inlet mass flux values in the core within the range of 1100-1300 kg/s where obtained. The heat transfer is improved while the mass flow in the core increases, the numerical results indicate that for 1,100 kg/s the temperature increase is greater than that for 1,200 and 1,300 kg/s, causing a relatively large increase on the coolant temperature in Channel 3.

Transient Analysis with Temperature feedback effects. The neutronic process, the heat transfer

in the fuel rod and the thermal-hydraulics in the core of the HPLWR were considered. The neutronic calculations were performed with the HELIOS-2 code and the obtained results were used to evaluate the reactivity due to fuel temperature and supercritical water density changes. Numerical analysis were obtained for two coolant transients in the core and the effects on power, fuel temperature, clad temperature and coolant density were presented. The maximum difference was found in the decreased mass flow coolant transient.

Finally the influence of the core inlet flow on the SCWR evaluated from the Monte Carlo simulation main results are,

- The simulation time required to reach steady state is 150 seconds when the core inlet flow varies ± 10% with respect to its nominal value.
- The simulation size required to have invariability is 5000.
- Invariability test concluded that the reactor core inflow is the output variable most sensitive to changes on the core inlet flow. Subsequently, the reactor power is the next most sensitive variable.
- Reactor power, fuel temperature and inflow to the core are directly proportional to the core inlet flow and have a linear correlation.

With the equations found with linear and square regressions, it is possible to predict the output variables of a SCWR by modifying the core inlet flow, which can be applied to operation and design of SCWRs.

REFERENCES

Barragán-Martínez A., 2013. Diseño neutrónico y termohidráulico de un reactor nuclear enfriado con agua supercrítica, PhD Thesis, Universidad Nacional Autónoma de México, Mexico City.

Barragán-Martínez A., Martin-del-Campo C., François J.-L., Espinosa-Paredes G., 2013. MCNPX and HELIOS-2 comparison for the neutronics calculations of a Supercritical Water Reactor HPLWR, Annals of Nuclear Energy, 51 181-188.

Bishop A., Sandberg R., Tong L., 1964. High Temperature Supercritical Pressure Water Loop: Part IV, Forced Convection Heat Transfer to Water at Near-Critical Temperatures and Super-Critical Pressures, Westinghouse Electric Corporation, Pittsburgh, Pennsylvania.

Cheng, X., Kuang, B., Yang, Y.H., 2007. Numerical analysis of heat transfer in supercritical water cooled flow channels. Nuclear Engineering and Design 237, 240-252.

Cheng, X., Schulenberg T., 2001. Heat transfer at supercritical pressure - literature review and application to a HPLWR. Scientific Report FZKA 6609.

Dittus F., Boelter L., 1930. Heat transfer in automobile radiators of the tubular type, University of California, Publications in Engineering, 2, 443-461.

Dobashi, K., Oka, Y., Koshizuka, S., 1998. Conceptual design of a high temperature power reactor cooled and moderated by supercritical light water. Annals of Nuclear Energy 25: 487–505.

Duderstadt J., Hamilton L., 1976. Nuclear Reactor Analysis. John Wiley & Sons, United States of America.

Espinosa-Paredes G., Espinosa-Martínez E.-G., 2009. Fuel rod model based on Non-Fourier heat conduction equation, Annals of Nuclear Energy, 36, 680-693.

Espinosa-Martínez E.-G., Martin-del-Campo C., François J. L., Espinosa-Paredes G., 2015. Effect of Heat Transfer Correlations on the Fuel Temperature Prediction of SCWRs. In: International Congress on Advances in Nuclear Power Plants, NICE, France.

Gallaway, T., Antal, S., Podowski, M., 2008. Multi-dimensional model of fluid flow and heat transfer in Generation-IV Supercritical Water Reactor. Nuclear Engineering and Design 238: 1909-1916.

Gu, H.Y., Cheng, X., Yang, Y.H., 2008. CFD analysis thermal-hydraulic behavior in SCWR typical flow channels. Nuclear Engineering and Design 238: 3348-3359.

Hofmeister J., Waata C., Starflinger J., Shulenberg T., Laurien E., 2007. Fuel assembly design study for a reactor with supercritical water, Nuclear Engineering and Design, 237, 1513-1521.

Hongzhi, L., Wang, H., Luo, Y., Gu, H., Shi, X., Chen, T., Laurien, E., Zhu, Y., 2009. Experimental investigation on heat transfer from a heated rod with a helically wrapped wire inside a square vertical channel to water at supercritical pressures. Nuclear Engineering and Design 239: 2004-2012.

McAdams W., 1942. Heat Transmission, 2nd ed., McGraw-Hill, New York.

Mokry S., Farah A., King K., Gupta S., Pioro I., Kirillov P., 2009. Development of supercritical water heat-transfer correlation for vertical bare tubes," International Conference Nuclear Energy for New Europe 2009, Slovenia.

Patankar S., 1980. Numerical Heat Transfer and Fluid Flow. McGraw-Hill, New York .

Quezada-García S., Espinosa-Martinez E.-G., Espinosa-Paredes G., and Vázquez-Rodríguez A., 2016. Power-feedwater temperature operating domain for a BWR driven by natural convection, Progress in Nuclear Energy 86: 110-119.

Pioro I., Khartabil H., and Duffey R., 2004. Heat transfer to supercritical fluids flowing in channels—empirical correlations (survey), Nuclear Engineering and Design, 230, 1, 69-91.

Pioro I., Duffey R., 2007. Heat Transfer and Hydraulic Resistance at Supercritical Pressures in Power Engineering Applications, ASME Press, New York.

Reiss T., Fehér S., Czifrus S., 2008. Coupled neutronics and thermohydraulics calculations with burn-up for HPLWRs," Progress in Nuclear Energy, 50, 52-61.

Renz, U., Bellinghausen, R., 1986. Heat transfer in a vertical pipe at supercritical pressure. In: 8th International Heat Transfer Conference 3: 957–962.

Schulenberg T., Starflinger J., 2007. Core design concepts for high performance light water reactors, Nuclear Engineering and Technology, 39, 249-256.

Shulenberg T., Starflinger J., 2012. High performance light water reactor. Design and analyses. KIT Scientific Publishing, Germany.

Schnurr N., Sastry V., Shapiro A., 1976. A Numerical Analysis of Heat Transfer to Fluids near the Thermodynamic Critical Point Including the Thermal Entrance Region, Journal of Heat Transfer, Transactions of the ASME, 98, 4, 609-615.

Starflinger, J., Schulenberg, T., Marsault, Ph, Bittermann, D., Laurien, E., Maraczy, C., Anglart, H., Lycklama, J.-A., Andreani, M., Ruzickova, M., Vanttola, T., Kiss, A., Rohde, M. and Novotny, R., 2010. Specific targeted research or innovation project, Contract No. FI6O-036230: High performance light water reactor Phase 2, Sixth framework programme.

Swenson H., Carver J., Kakarala C., 1965. Heat Transfer to Supercritical Water in Smooth-Bore Tubes, Journal of Heat Transfer, Trans. ASME Series C, 87, 4, 477-484.

Thind H., 2012. Heat-transfer analysis of double-pipe heat exchangers for indirect-cycle SCW NPP, Master Thesis, University of Ontario Institute of Technology, Ontario.

Wagner W., Kretzschmar H.-J., 2008. International Steam Tables. Properties of Water and Steam based on the Industrial Formulation IAPWS-IF97, Springer, Second Edition.

Zhu D., Tian W., Zhao H., Su Y., Qiu s., Su G., 2013. Comparative study of transient thermal–hydraulic characteristics of SCWRs with different core design. Annals of Nuclear Energy 51: 135-145.